HEAT INPUT EFFECT ON MECHANICAL AND CORROSION CHARACTERISTICS OF MIG-WELDED JOINT WELDS IN PETROLEUM STORAGE TANKS

2023
MASTER THESIS
MECHANICAL ENGINEERING

Hyder Abed Alrazzaq Ajeel AL-EETHAWI

Thesis Advisors
Assist. Prof. Dr. Khaled M.N. CHAHROUR
Prof. Dr. Abbas Sheyaa ALWAN

HEAT INPUT EFFECT ON MECHANICAL AND CORROSION CHARACTERISTICS OF MIG-WELDED JOINT WELDS IN PETROLEUM STORAGE TANKS

Hyder Abed Alrazzaq Ajeel AL-EETHAWI

Thesis Advisors

Assist. Prof. Dr. Khaled M.N. CHAHROUR

Prof. Dr. Abbas Sheyaa ALWAN

T.C.

Karabuk University

Institute of Graduate Programs

Department of Mechanical Engineering

Prepared as

Master Thesis

KARABUK

November 2023

I certify that in my opinion the thesis submitted by Hyder Abed Alrazzaq Ajeel AL-EETHAWI titled "HEAT INPUT EFFECT ON MECHANICAL AND CORROSION CHARACTERISTICS OF MIG-WELDED JOINT WELDS IN PETROLEUM STORAGE TANKS" is fully adequate in scope and in quality as a thesis for the degree of Master of Science.

Assist. Prof. Dr. Khaled M.N. CHAHROUR .....

Thesis Advisor, Department of Mechanical Engineering

Prof. Dr. Abbas Sheyaa ALWAN .....

Thesis Advisor, Department of Mechanical Engineering

This thesis is accepted by the examining committee with a unanimous vote in the Department of Mechanical Engineering as a Master of Science thesis. 10/11/2023

Examining Committee Members (Institutions)	Signature
Chairman : Assist. Prof. Dr. Khaled M.N. CHAHROUR (KBU)	.....
Member : Prof. Dr. Abbas Sheyaa ALWAN (MTU)	.....
Member : Assoc. Prof. Dr. Daver ALİ (KBU)	.....
Member : Assoc. Prof. Dr. Harun ÇUG (KBU)	.....
Member : Assist. Prof. Dr. Sameer Khalaf FAYYADH (UOB)	.....

The degree of Master of Science by the thesis submitted is approved by the Administrative Board of the Institute of Graduate Programs, Karabuk University.

Assoc. Prof. Dr. Zeynep ÖZCAN .....

Director of the Institute of Graduate Programs

“I declare that all the information within this thesis has been gathered and presented in accordance with academic regulations and ethical principles and I have according to the requirements of these regulations and principles cited all those which do not originate in this work as well.”

Hyder Abed Alrazzaq Ajeel AL-EETHAWI

ABSTRACT

M. Sc. Thesis

HEAT INPUT EFFECT ON MECHANICAL AND CORROSION CHARACTERISTICS OF MIG-WELDED JOINT WELDS IN PETROLEUM STORAGE TANKS

Hyder Abed Alrazzaq Ajeel AL-EETHAWI

Karabük University
Institute of Graduate Programs
The Department of Mechanical Engineering

Thesis Advisors:
Assist. Prof. Dr. Khaled M.N. CHAHROUR
Prof. Dr. Abbas Sheyaa ALWAN
November 2023, 86 pages

The point of this study was to look at what happens to the microstructures, mechanical properties, and corrosion behavior of Metal Inert Gas (MIG) weld V joints in four AISI 1018 plates when different amounts of weld heat are added. Using a scanning electron microscope (SEM), the microstructure of two different areas was looked at: the fusion zone (FZ) and the heat-affected zone (HAZ) in all samples of AISI 1018 plates. A Vickers microhardness tester was used to measure the microhardness of the MIG weld joints in four samples of AISI 1018 plates. This was done to see how different areas affected the mechanical parameters. Four pieces of AISI 1018 steel plates were put through tension tests to determine their tensile and yield strengths at MIG-welded joints. The study investigates the link between how much heat is used during welding and the mechanical properties of the welded parts.

It was noticed that sample number 3 had diminished mechanical features. The electrochemical polarization test was used in this study to investigate the corrosion rating method. Four pieces of AISI 1018 plates were polarized to investigate the corrosion processes that control important parts of MIG weld joints. The tests were done in a solution that had lost all its air and had a density of 7.82 g/cm^3 and an equivalent weight of 27.89 g. It also had 1.5% NaCl in it. An important part of the final test is using X-ray diffraction (XRD) to look at the structure of crystalline substances. In this case, the researcher is looking at the different iron phases inside the mineral AISI 1018.

According to the results of this study, the MIG weld joints make sample number 3 more resistant to corrosion and make it more resistant to corrosion than the other samples. A higher heat input, specifically at a critical value of 1.286 KJ/mm, was used on sample 3. This caused both hardness and tensile strength to be lower compared to when a smaller heat input was used. Furthermore, the corrosion resistance was improved because more austenitic phases were formed, caused by the large rise in heat input. Because of this, it is suggested to use a lot of heat to keep the corrosion protection and make the welded joints stronger.

Key Words : Weld Heat Input, AISI 1018, Mechanical Properties, Corrosion Behavior, Weld Joint, MIG Welding, Tensile Strength, Hardness, Corrosion Resistance, Welding Process Optimization.

Science Code : 91511

ÖZET

Yüksek Lisans Tezi

PETROL DEPOLAMA TANKLARINDA MIG KAYNAKLI BİRLEŞİM KAYNAKLARININ MEKANİK VE KOROZYON ÖZELLİKLERİNE ISI GİRİŞİNİN ETKİSİ

Hyder Abed Alrazzaq Ajeel AL-EETHAWI

Karabük Üniversitesi
Lisansüstü Eğitim Enstitüsü
Makine Mühendisliği Anabilim Dalı

Tez Danışmanları:
Dr. Öğr. Üyesi Khaled M.N. CHAHROUR
Prof. Dr. Abbas Sheyaa ALWAN
Kasım 2023, 86 sayfa

Bu çalışmanın amacı, farklı miktarlarda kaynak ısısı eklendiğinde dört AISI 1018 plakadaki Metal İnert Gaz (MIG) kaynak V bağlantılarının mikroyapılarına, mekanik özelliklerine ve korozyon davranışına ne olduğuna bakmaktı. Taramalı elektron mikroskobu (SEM) kullanılarak iki farklı bölgenin mikroyapısına bakılmıştır: AISI 1018 plakaların tüm numunelerinde füzyon bölgesi (FZ) ve ısıdan etkilenen bölge (HAZ). AISI 1018 plakalardan alınan dört numunedeki MIG kaynak bağlantılarının mikrosertliğini ölçmek için bir Vickers mikrosertlik test cihazı kullanılmıştır. Bu, farklı alanların mekanik parametreleri nasıl etkilediğini görmek için yapıldı. Dört adet AISI 1018 çelik plaka, MIG kaynaklı bağlantılardaki çekme ve akma dayanımlarını belirlemek için çekme testlerine tabi tutulmuştur. Çalışma, kaynak sırasında ne kadar ısı kullanıldığı ile kaynaklı parçaların mekanik özellikleri

arasındaki bağlantıyı araştırmaktadır. Numune 3'ün mekanik özelliklerinde azalma olduğu görülmüştür. Bu çalışmada korozyon derecelendirme yöntemini araştırmak için elektrokimyasal polarizasyon testi kullanılmıştır. MIG kaynak bağlantılarının önemli kısımlarını kontrol eden korozyon süreçlerini araştırmak için dört adet AISI 1018 plaka polarize edilmiştir. Testler, tüm havasını kaybetmiş, 7,82 g/cm3 yoğunluğa ve 27,89 g eşdeğer ağırlığa sahip bir çözelti içinde yapılmıştır. Son testin önemli bir kısmı, kristal maddelerin yapısına bakmak için X-ışını kırınımını (XRD) kullanmaktır. Bu durumda araştırmacı, AISI 1018 mineralinin içindeki farklı demir fazlarına bakmaktadır.

Bu çalışmanın sonuçlarına göre, MIG kaynak bağlantıları 3 numaralı numuneyi korozyona karşı daha dirençli hale getirmekte ve diğer numunelere göre korozyona karşı daha dayanıklı olmasını sağlamaktadır. Numune 3'te özellikle 1.286 KJ/mm kritik değerinde daha yüksek bir ısı girdisi kullanılmıştır. Bu, hem sertliğin hem de çekme mukavemetinin daha düşük bir ısı girdisinin kullanıldığı duruma kıyasla daha düşük olmasına neden olmuştur. Ayrıca, ısı girdisindeki büyük artış nedeniyle daha fazla östenitik faz oluştuğu için korozyon direnci iyileşmiştir. Bu nedenle, korozyon korumasını korumak ve kaynaklı bağlantıları daha güçlü hale getirmek için çok fazla ısı kullanılması önerilmektedir.

Anahtar Kelimeler : Kaynak Isı Girdisi, AISI 1018, Mekanik Özellikler, Korozyon Davranışı, Kaynak Birleşimi, MIG Kaynağı, Çekme Mukavemeti, Sertlik, Korozyon Direnci, Kaynak İşlemi Optimizasyonu.

Balam Kodu **:** 91511

ACKNOWLEDGMENT

In the beginning, thank God. No one can help you more than Allah. I would not be where I am now without His kindness. Many thanks to my mother, who gave up a lot for me and loved me as a child while she cared for me and as a young man while she prayed for me, my late father, my dear brothers, and my wife, who always supported me in school and life.

Special thanks and respect to my bosses, Assist. Prof. Dr. Khaled M. N. CHAHROUR and Prof. Dr. Abbas Sheyaa ALWAN, for all the help, support, understanding, and kindness they showed me.

CONTENTS

Page

Page

Page

LIST OF FIGURES

Page

Page

LIST OF TABLES

Page

SYMBOLS AND ABBREVITIONS INDEX

SYMBOLS

ρ : Density of Metal or Alloy

η : Weld Heat Transfer Efficiency

ABBREVITIONS

MIG : Metal Inert Gas

MAG : Metal Active Gas

GMAW : Gas Metal Arc Welding

WFS : Wire Feed Speed

HAZ : Heat-Affected Zone

FZ : Fusion Zone

Amps : Amperes

DOE : Design of Experiments

BH : Bead Height

BW : Bead Width

ASME : American Society for Testing and Materials

V : Voltage

A : Amperes

KN : Kilonewton

MPa : Megapascal

SEM : Scanning Electron Microscope

ASTM : Average Linkage Cluster Analysis

HV : Hardness Vickers

AISI : American Iron and Steel Institute

i_{corr} : Corrosion Current Density

WZ : Welding Zone

C.R : Corrosion Rate

CHC : Characteristic-Hardness Curve

CCT : Continuous Cooling Transformation

C.E. : Carbon Equivalent

W : equivalent weight

WM : Weld Metal

BM : Base Metal

PART 1

INTRODUCTION

A variety of welding techniques, including MIG/MAG, TIG, and LASER, have been invented over the years. These procedures have been enhanced, particularly in the ongoing quest to boost productivity.

There is a belief in the technical community that the process that results in the highest melting frequency of additional material yields the highest productivity. For instance, almost universal agreement exists that the MIG/MAG operation and the TIG process differ significantly in terms of the melt rate of additional material. This claim is contested on two different fronts. First, only if the exact same current is applied can the MIG or MAG achieve a higher fusion rate. The Tig as well as MIG and MAG procedures are comparable when the margin is given at the same power [1]. Second, the LASER process's productivity for root application, which it even reaches if requested without introducing any additive material, would not be justified under this feature of fusion rate.

Therefore, it is important to consider other factors in addition to melting rates while evaluating productivity. It should not be evaluated using such a constrained examination but rather using far broader criteria. The number of finished goods with the requisite quality and requirements is what matters, not how much fusion rate or penetration capacity a method has. For this reason, it is vital to combine the desired penetration profile with the melting rate as needed [2].

The amount of downtime that operations experience is another crucial factor for productivity. This final point is especially crucial in the context of orbital welding because the various relative locations of the welding flame place unique constraints on each procedure. For instance, the MIG/MAG process lacks the ability to

geometrically meet the weld joint if the orbit continues the same welding path since it alternates between the downward and upward vertical positions. For the technique described above, this results in welds with distinctly varied geometry. The TIG technique contemplates the capability of continuing without welding while pausing, running a full orbit; thus, this no longer occurs in the same way [3].

Hence, despite the wide range of alternatives and the progress in the improvement of welding forms, the hunt for enhancements that can contribute to greater productivity, robustness, and reduction of the disappointment rate could be of extraordinary interest to the industry within the Brazilian and universal setting. This paper presents the advancement of an orbital TIG welding adaptation with uncommon consideration for efficiency assessment.

1.1. WELDING TECHNIQUES

Welding is a method that has been used for a long time to join and seal off gaps between two pieces of the same or varied types of material. Arc welding is one of the most popular ways to join things together because it can be used in many different fields. This method is very complicated, which makes it hard for businesses to use and lowers their output. Most industries' main goal is to make the economy more productive. To solve the problems with arc welding, we need new technologies for the way we do things now. As technology has improved, welders can now use new power sources that give them more precise control over process variables. As a result of this change, the number of process parameters has grown, which means there are now more things to look into. Cause-and-effect studies and the ability to use computers have helped guide welding research. Even though the number of variables in the process has grown, the stability of the process has remained a major concern. When a higher deposition is needed, the traditional single-wire method has problems, such as taking longer to weld, using more material, and being less productive. Multiple-wire welding was made to get around these problems and increase production [4].

1.2. WELDING USING MIG

To perform MIG or MAG welding, it is imperative to supply an electric current to the torch. This phenomenon results in the initiation of an explosion at the interface of the supplied wire and the workpiece undergoing welding. The arc will cause the wire and the material being welded to undergo a melting process, resulting in their fusion into a unified entity. The wire feeder exhibits a continuous motion to supply welding wire into the welding torch while it traverses the burner. The provision of shielding gas utilized in welding is attributed to the flame itself. In contrast to MAG (Metal Active Gas) welding, in which the shielding gas really plays an active role and contributes significantly to the welding process, MIG (Metal Inert Gas) welding uses a shielding gas that is inert and does not actively engage in the welding process. MAG welding is frequently preferred over MIG welding due to the prevalent utilization of compressed air comprising granular activated carbon dioxide or oxygen. The phrases MIG welder and MAG welder are frequently used interchangeably due to a prevailing lack of clarity and comprehension [5].

Basic components of MIG and MAG welding equipment include power sources, wire feeders, ground cables, welding torches, and optional cooling systems, as well as shielding gas tanks or gas mains interfaces. It is possible to move the coil of welding wire from the workstation to the torch with the assistance of the wire feeder. The wire feeder, which makes use of power electronics supplies, is responsible for starting and stopping the power supply as well as regulating the voltage. In order to achieve this goal, a control cable is connected between the power source and the wire feeder. In addition to this responsibility, the wire feeder is in charge of regulating the release of the shielding gas. It is possible to collect welding shielding gas from either storage facilities or piped-in supply lines. Both options are available. The MIG welding equipment offered by Kemppi is extensively configurable, with individual cooling and power modules as well as wire feeders available for purchase. Since the only component of the welder that needs to be moved from one location to another is the wire feeder, the rest of the welder can remain in place while the operator commutes between different jobs. Additionally, certain versions may incorporate control panels that can be removed and additional functionality that can be activated

in a standalone fashion. Due to the fact that the welding process causes the torch to get hot, it is necessary to employ either a gas or a liquid in order to cool it. Gas-cooled torches are so-called because they employ a shielding gas that also functions as a coolant. For welding torches that require liquid to be pushed through the welding cable, separate liquid cooling units are required. This equipment must be purchased separately. The shape of MIG and MAG welding equipment is constrained by the wire coils that are utilized in the equipment. Because of their length, coils are typically awkward and difficult to work with due to their bulk. The most cutting-edge MIG/MAG welding equipment, on the other hand, consists of compact and lightweight devices like the Kemppi MinarcMig Adaptive 180, which was the winner of the 2006 Red Dot Award [6].

1.3. MIG WELDING TECHNOLOGY

The welding torch is used in both metal-inert-gas and metal-arc welding. Its job is to feed the workpiece with the welding wire, shielding gas, and necessary welding current. Position, torch angle, wire plug output, welding speed, and weld pool form are the most critical factors to consider while MIG or MAG welding. As the torch carrying the arc is steadily moved along the welding bevel, the arc is ignited by means of a trigger. Molten welds must be watched as they form. Maintain a steady distance and angle between the welding torch and the workpiece. Focusing on the molten weld is crucial. Soldering errors are more likely to occur during a period of inattention. In such a circumstance, it is best to pause welding for a short period of time before restarting [2].

1.4. PROCESSES FOR MIG WELDING

Metal inert gas (MIG) welding is also known as gas metal arc welding (GMAW) and by a few other names. As the weld's filler material, the disposable wire electrode is used with the arc's shielding gas to strengthen the weld, deepen its penetration, and reduce the weld bead's porosity.

The welding gun (or torch) serves as a conduit for both the electrode and the shielding gas, which originate from distinct locations. Commonly used shielding gas mixtures for steel welding include 75% argon and 25% carbon dioxide. The materials being welded, and other factors, may dictate the use of different mixes.

A conduit (also known as a torch) transports a consumable wire electrode and shielding gas to the welding gun. When it comes to welding, the type of metal, as well as its thickness and configuration, all play a part in deciding the composition of the electrode wire, as well as its diameter [4]. The amount of metal that is deposited at the joint is determined by how quickly the electrode is supplied into the weld, which is controlled by the wire feed speed (WFS) [7].

1.5. OBJECTIVE OF THE WORK

The objectives of the current work are to:

1. This study aims to investigate the influence of heat input on the mechanical characteristics and microstructure of V-single butt joint welds in metal type AISI 1018. The welding process employed in this research is Metal Inert Gas (MIG) welding, and various welding parameters are considered for analysis.
2. The purpose of this research is to identify the optimum weld parameters, particularly heat input, that produce the best results in terms of the mechanical properties of elements, namely microhardness and tensile strength.
3. The purpose of this research is to learn how much heat is used during welding affects how well the welds hold up against corrosion.
4. The purpose of this research is to examine the effect of weld heat input on the structure of Widmanstatten, acicular, and allotropic ferrite in the Fusion Zone (FZ) and Heat Affected Zone (HAZ) regions.

LAYOUT OF THE WORK

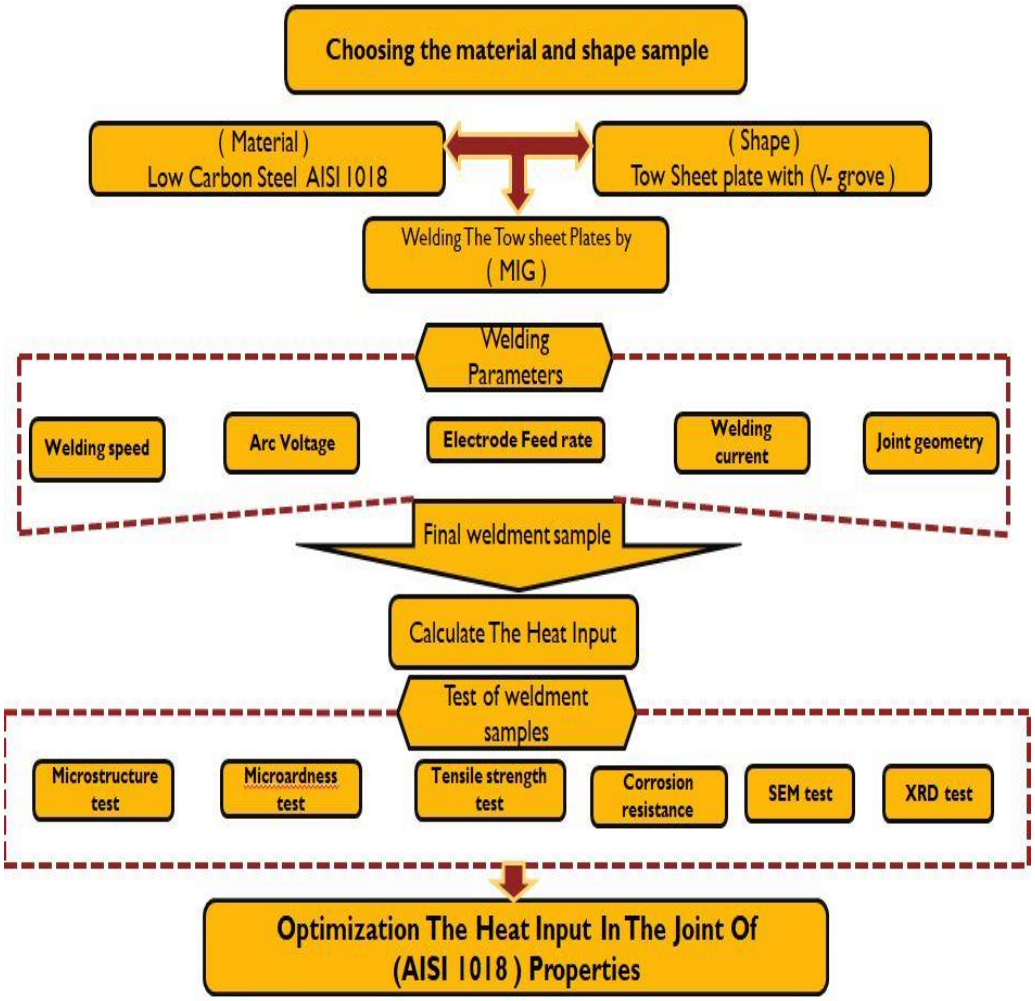

Figure 1.1. Layout of work.

PART 2

LITERATURE REVIEW

Over the years, researchers have directed their attention towards the heat sink and its optimization, driven by the increasing prevalence of electronic devices and the need for effective cooling mechanisms. Water, air, and nanofluids are the three predominant fluid mediums employed for heat transfer in heat sinks. This section provides an overview of the literature review conducted for the present study.

Recent decades have seen a resurgence of interest in the concept of heat sinks as a result of the proliferation of electronic gadgets and its application in engineering. In order to effectively address the challenge of managing significant heat emissions within the constraints of limited resources and spatial limitations, it is imperative to develop novel solutions that demonstrate proficiency in this regard. Finned heat sinks are widely recognized as a highly efficient approach for managing and dissipating heat.

2.1. PRIVIOUS STUDIES

Kausar et al. [8], A strong bond between two different kinds of metal is made when its strength is the same as that of the metal that is weaker of the two. Combinations of SS 316L and IS 2062 are often used in heat exchangers, superheaters in oil gasification plants, chemical processing equipment, and the nuclear industry. Due to the different thermal and mechanical properties of the materials being joined in a normal welding setting, it has been hard to successfully weld metals that are not the same. As time has gone on, joints that weren't up to par have caused the lives of many machines to shorten or not match up with what was expected. The joints might not be as strong as they should be because the welding methods used during the making process were not good enough. There are many problems that can happen

during different welding processes, such as splitting, large residual stresses in welds, atom migration that leads to stress concentration, and stress corrosion cracking. To deal with these problems, it is important to do a full study of how different welding process parameters affect each other. The main goal of this project is to find out more about how Tungsten Inert Gas (TIG) welding affects the mechanical qualities of SS 316L and IS 2062 alloys. Using Taguchi and Analysis of Variation (ANOVA) methods, the project also wants to find the best process parameters. Lastly, the microstructural qualities of the materials that were joined together were looked into. This method makes a larger-scale weld that is cleaner and purer. The goal of this study is to find out how different welding currents (110, 120, and 130 Amps), voltages (40, 50, and 60 Volts), and gas flow rates (8, 9, and 10 Liters per minute) affect the final tensile strength and hardness of welds made from different types of metal. The Design of Experiments (DOE) method will be used to figure out how important these input factors are. The main goal of this study is to look into how Tungsten Inert Gas (TIG) Welding works with different materials, especially SS 316L and IS 2062. The goal is to test the hardness of the welded parts and then use Analysis of Variance (ANOVA) to look at the results. The Taguchi method will also be used to improve the process of optimization. A microstructural study will also be done to get a better idea of how the welded joints work.

In Kadephi V. et al. [9], Sheets of super duplex stainless steel with a UNS S32750 grade were welded at energies of 0.54 and 1.10 kJ/mm using an E2595 electrode. Investigations into the microstructure of the heat-affected zone using optical and scanning electron microscopy revealed only minor differences between the two heat inputs. The weld metals had Widmanstatten austenite and ferrite, as well as austenite and ferrite at the intra-granular and grain boundary levels. The amount of ferrite present in the weld region was not significantly altered by the addition of heat. Despite having similar mechanical qualities (tensile strength, impact strength, and hardness), the welds broke ductilely in both cases. Experiments in 3.5% NaCl showed that both heat sources had nearly the same pitting potential, and that sensitization was less than 1%. Welding UNS S32750 super duplex stainless steel may benefit from a reduced heat input, as we found that doing so had no effect on the weld's behavior.

Bandhu et al. [10], Pipeline welding is becoming more and more important, especially in terms of quality, and more and more modern materials that are sensitive to heat and corrosion are being used. High production costs also mean that the welding process needs to be looked at in depth. In order to deal with these problems, it is important to use highly advanced welding methods that combine modern power sources and complex software configurations. Regulated Metal Deposition (RMDTM) welding is one method that can be used. In the given situation, this study looks at how the factors of regulated metal deposition (RMDTM) welding affect ASME SA387-11-2 steels. Controlling the current (A), voltage (V), and gas flow rate (GFR) are important parts of the regulated metal deposition (RMDTM) welding method that is most often used. Bead height (BH), bead width (BW), heat-affected zone (HAZ), and depth of penetration (DOP) are all metrics used to evaluate the procedure's efficacy. We also consider the Rao method for welding optimization. It was determined that 92 A of current, 13 V of voltage, and 21 L/min of gas flow produced the greatest results during welding. The effectiveness of the strategy is demonstrated by a comparison to the JAYA and teaching learning-based optimization (TLBO) approaches.

Richard et al. [11], Ferritic cryogenic steels are a type of low-alloy steel that contains nickel and is designed to work safely at temperatures much lower than 0°C. These steels stand out because they have good tensile qualities and high impact strength, even when they are cold. Usually, the amount of nickel in carbon-manganese steels ranges from about 1.5% to 9%. But it's important to keep in mind that some fine-grained carbon-manganese steels can work at temperatures as low as -50°C. The steel types listed above are often used in the oil and gas and petrochemical industries. They are used to handle and store liquid petroleum gases (LPG) at temperatures as low as -100°C. When it comes to 9% nickel steel, it can handle temperatures as low as -196°C. Also, these machines can be found in the gas processing industry, where they are used to make and control different gases, like carbon dioxide and oxygen.

Vikas et al. [12], Titanium and its alloys find widespread use in a variety of industries, including transportation, aircraft, and healthcare. Fusion bonding of titanium presents a number of difficulties. Titanium components can also be joined

without any defects using a process called friction welding. In this study, Ti-6Al-4V Grade 5 titanium alloy bars were welded using a rotary friction process. The welding procedure began with the preheating and subsequent tension release of rods made of Grade 5 titanium alloy. In addition, some rods went through a stress-relieving process after the welding was done to ensure the best possible results. Friction welding at a rotational speed of 1500 revolutions per minute (rpm) with an applied force of 5 kilonewtons (kN) was found, after numerous trials, to result in the production of joints with no defects. Because of the heat treatment, the metal is more malleable than before. The use of heat treatment resulted in the formation of a bimodal microstructure in the primary metal, while a lamellar microstructure was seen as a consequence of the heat treatment. The coarse grains exhibit the presence of clusters of molds inside their structure. Of the several heat treatment conditions evaluated, the stress relief condition exhibited the greatest hardness. The improvement in hardness of the welds can be attributed to the formation of precipitates, which resulted from the reduction of stress levels. In settings where treatment has been applied, the crack exhibits a stiff shape, whereas in conditions where no treatment has been administered, the fracture displays a flexible shape. Regardless of the heat treatments employed, each of the welding specimens exhibited fracture at the weld joint. This observation indicates that the weld region exhibits significantly greater strength compared to the base region, mostly because to the presence of acicular microstructures and distinct phases. The analysis of microstructural characteristics revealed a significant correlation between mechanical qualities.

Chujutalli et al. [13], The numerical modeling of welding encompasses thermal and mechanical evaluations, along with metallurgical issues. Thermal analysis is employed to ascertain the temporal evolution of temperature within the welded component. Ensuring the precision of this data holds significant importance in facilitating subsequent investigations pertaining to the structural integrity of steel-plated structures, particularly in relation to buckling and fatigue failure modes. Goldak's parameters—which are represented as a dual ellipsoid shape—greatly affect how heat is distributed, as do the source's dimensions and configuration. The fundamental difficulty arises from the fact that modifying these parts sometimes

requires a trial-and-error approach in order to get an acceptable temperature distribution. In order to better understand the impact of Goldak's parameters on the weld bead dimensions in 2D and 3D numerical welding models, this study presents a parametric evaluation. This research suggests a method for calculating the parameters of a double ellipsoid-shaped portable heat source. An algorithm has been developed by integrating analytical formulation, experimental data, and numerical simulation. The isotherms are determined using Fachinotti's analytical approach. The isotherm of the material's melting temperature provides valuable insights into the optimal size of the weld beads. The algorithm is provided with empirical data, encompassing the variables associated with the welding process and the dimensions of the weld bead. In order to validate and establish the efficacy of the approach, computational models have been developed to simulate the welding process.

In Qin et al. [14], Welding tests and a computerized model analysis of the various magnesium alloys, AZ61–AM60, were conducted using TIG and A-TIG. A three-dimensional mathematical model of a welding pool with a moving heat source has been created, and a numerical simulation of the temperature field has been performed. The impact of welding process parameters on the surface quality of welded connections has been discussed. The modeling findings demonstrate that neither the shape distribution of the melting field nor the temperature field distribution of the various magnesium alloys (AZ61-AM60) during the TIG welding process are the same on both sides of the molten pool. The surface of the melted pools takes on the shape of an ingot when A-TIG welding is performed with an active flux. Experiments verify the outcomes of these simulations. The agreement between the modeling and experiment data demonstrates the geometry of the pool of molten metal during the welding process, as well as the variation law of the temperature field. This is a useful method for determining how to best optimize the parameters of the welding process for various magnesium alloys.

Garcia et al. [15], Investigations were conducted on the corrosion of joints made of high-strength steel at a strength of 900 MPa following welding with metal-active gas. The weld was produced using two heat sources. Potentiodynamic polarization tests and electrochemical impedance spectroscopy were used to investigate corrosion in

3.5 weight percent NaCl. It was discovered using microstructural (WM) investigation with optical, checking electrons, and transmission electron microscopy to determine that the weld metal and HAZ were different from each other. Confocal laser scanning microscopy was used to measure the thickness of HAZ and WM both before and after corrosion. It was discovered that adding heat had no effect on the corrosion of HSLA steel. Anodic and cathodic joint depths can differ. In the WM, it is cathodic, while in the HAZ, it is anodic. Corrosion was affected by the amount and configuration of carbides within the Hazardous area zone. There was martensite and bainite in the HAZ, but circular fer rite was the weld metal.

Shuai et al. [16] SevenN01-T5 alloy (AT5) and SevenN01-T4 alloy (AT4) were found to be combined by metal inert gas (MIG) the welding process using ER5356 filler wire. The main goal of the study was to examine the mechanical characteristics and corrosion resistance of the welded joint. The mechanical properties of welded junctions are inferior to those of base metals (BMs). Because of the presence of copper (Cu), zinc (Zn), and precipitates at varying concentrations in the weld, there is a possible distinction between the AT5 and AT4 sides of the joint that was welded, which leads to galvanic corrosion. On the AT4 side, the vicinity of the weld zone was more prone to corrosion.

Adewuyi et al. [17], The impact of heat from welding on the mechanical characteristics of steel was examined. A flat bar made of ASTM A304 stainless steel that had a thickness of 5.0 millimeters was used as the test specimen for the weld. Type K thermocouples were inserted into each hole to track the temperatures of the welds. Three of the MIG welding parameters were changed while the sample was being produced. The variables that are modifiable in this situation are the welding current, the number of passes, and the thermocouple's position in the middle of the weld. The length of time that may be spent on an experiment was limited by Taguchi's L9 array (DOE). To find out how much the weld heat had impacted the samples, a series of microstructural and mechanical tests were performed on them. The test findings showed that a higher percentage of weld runs on the base metal and the HAZ were necessary to obtain a lower hardness. Tensile strength tests on samples 80A and 100A showed that strength increased with more weld passes, but

sample 60A's test findings showed that strength decreased. It was feasible to create a structure with more impact resistance by carrying out extra weld passes. The portions of a weld that achieve a particular peak temperature throughout the process of welding spread outward from the weld center, depending on the amount of heat delivered to the weld. The temperature fields enlarge as the heat source heats the thermocouple's cross-section. The temperature starts to decrease as time goes on. When there is more space between a thermometer and the weld, the temperature of the weld will start to rise.

Ylmaz et al. [18], The utilization of welding techniques with the aluminum alloy AA6061-T6 is prevalent in various industries, including construction, automotive, and rail, owing to the material's exceptional resistance to corrosion, low density, and impressive strength-to-weight ratio. During the course of this study, the utilization of ER5356 filler wire via an automated system was employed to perform welding on AA6061-T6. The researchers conducted an investigation on the weld's macrostructure, microstructure, and mechanical properties. They examined the impact of different shielding gas conditions, specifically argon and helium, on the hardness and tensile strength. The impermeability of welds can be enhanced through the utilization of helium gas. The introduction of helium gas into the welding process resulted in a significant enhancement in the strength of the weld, with an increase from 190 MPa to 221 MPa. The tensile strength of the welded joints, which varied between 190 and 221 MPa, exhibited a notable decrease compared to that of the underlying material. The observed phenomenon can be attributed to the thermal cycle experienced during the welding process, resulting in an increase in grain size within the heat-affected zone, reaching a magnitude of 290 MPa. Dendritic, columnar, and coarse grains were found in both the partially melted zone and the heat-affected zone of the weld bead. The aforementioned regions remained unaltered by the shielding gas; nonetheless, the introduction of helium resulted in an augmentation of the heated surface area. The transition from the weld region to the base material resulted in an increase in the cross-sectional hardness from sixty to ninety HV. The ideal microhardness, mechanical characteristics, and cost are observed in gas mixtures containing 25% argon and 75% helium.

Pradip et al. [19], In this investigation, the quantity of heat applied has a correlation with the quality of the Tungsten inert gas (TIG) weld. The Tungsten Inert Gas (TIG) welding procedure used three different heat settings: low (0.75 kJ/mm), medium (0.90 kJ/mm), and high (11.05 kJ/mm). Austenitic 316L stainless steel needed to be welded, hence these heat sources were needed. The procedure makes use of semiautomatic Tungsten Inert Gas (TIG) welding equipment. The metallurgical and mechanical properties of the joints are examined, and the shape of the weld bead is examined in proportion to the heat applied. It has been observed that when the heat input is increased, the weld bead's diameter increases and its height decreases. Heating the material can increase its hardness and tensile strength, but only to a limited extent. Thus, there is a drop after. The study indicated that joints created with medium heat input had higher tensile strength, yield strength, percentage elongation, and microhardness values than joints made with low heat input. Because of the reduced dendritic spacing and dendritic size in the weld territory, a very tiny skeletal ferrite is produced inside a homogeneous austenitic matrix, causing the phenomenon. The SEM fractography of a joint created with a medium heat input reveals the presence of several small pits that are only a few microns deep.

Moi et al. [19]. At the time of the 36th century, 2022, Michel was an elf. The use of robots to assist in juncture wire and arc additive manufacturing could allow for the production of more complex nodes, space trusses, and grid shells at a higher rate of productivity. The mechanical and physical properties of these materials are excellent for use in structural applications; however, it is unknown how long these materials will remain in use. Low-carbon steel bars that have been manufactured additively, point-by-point, utilizing wire and arc technology are subjected to corrosion testing. The microstructure of the steel bars reveals their consistency, which is exactly what a metalworker would anticipate finding. Concave areas are the first to show signs of corrosion, as demonstrated by tests designed to simulate atmospheric exposure. Microscopy and electrochemistry, respectively, were used to investigate the post-printing cleaning process and surface state of the material. In laboratory experiments, it was found that oxide scales from wire manufacturing and arc additive manufacturing both influenced the corrosion of steel. If low-carbon steel components made through wire and arc additive manufacturing are going to be used for an

extended period, then the geometry and surface state of those components need to be given a great deal of consideration. In this study, the durability of low-carbon steel bars created by wire and arc Additive Manufacturing (AM) is investigated. Investigations are being done into the effects of corrosion. When it comes to the long-term use of wire and arc synergistically able to produce low-carbon steel components, geometry and post-print cleaning are two aspects that are absolutely essential.

Zainuddin et al. [20-22] Microstructure, mechanical properties, and corrosion behavior of friction stir welded (FSW) AA6061 aluminum alloys were the primary focus of this study. Grain sizes varied noticeably between the nugget zone, the zone that had been thermomechanically impacted, the zone that had been heated, and the base material. The HAZ material was the softest, while the BM substance was the hardest. Throughout the tensile testing process, cracks showed up in the transitional area between the TMAZ and the HAZ. Corrosion resistance of AA6061-AA6061 and the heat-affected zone (HAZ) was improved by using the friction stir welding (FSW) technology, as shown by polarization testing. According to Raman analysis, Al underwent a transition that led to the creation of aluminum hydroxide upon contact with water. New Zealand (NZ) and bottom intergranular attacks were found during scanning electron microscopy (SEM) investigation.

Qin and Hua, 2021 [23], Metal active gas arc welding was used to join pieces of high-strength low-alloy (HSLA) steel (MAG). Optical microscopy (OM), scanning electron microscopy (SEM), potentiodynamic polarization curves, and electrochemical impedance spectroscopy were used to study the effect of heat input on the microstructure and corrosion behavior of HSLA welds. The amount of acicular ferrite (AF) in the weld first goes up and then down as heat is added. At 11.9 kJ cm1, the amount of AF is at its highest. How the weld metal reacts to corrosion depends a lot on the type of microstructure. In a 3.5 wt% NaCl solution, adding more acicular ferrite can make corrosion worse. Weld metal corrosion is also affected by how thick and dense the corrosion products are on sample surfaces. When the corrosion product is loose, porous, and broken, it doesn't protect the weldmetal very well and speeds up its rate of corrosion.

Hussein 2020 [24], Current research examines how low-carbon steel 1020 AISI welded joints corrode when DC current and voltage change. Some welded joints are shot-peened with steel balls before welding, then welded without shot-peening. ASTM has made 15x15x3mm corrosion inspection samples (G71-31). All samples were electrochemically tested for microstructure, residual stress, and corrosion in 3.5% NaCl. The Tafel equation calculated the corrosion rate. Some welded joints show higher corrosion than others, as does the base metal. Because input current heat varies from pass to pass. Welded joints without shot peening had a higher corrosion rate due to residual compression stresses. Reduce weld passes and welding current to get enough heat.

Bansod et al. [25], We investigated, using the 308L electrode, how the welding process affected the metallurgical, mechanical, and corrosion behavior of gas tungsten arc welding rather than shielded metal arc welding. Specifically, we looked at how the welding process affected gas-tungsten arc welding. When the grains were equiaxed, the welds that were made from tungsten inert gas saw increases in both their hardness and their tensile strength. In shielded metal arc welding, both the heat-affected zone and the unmixed zone are significantly larger in comparison to tungsten inert gas welding. Both the length of dendrites and the distance between them can be reduced through the use of tungsten inert gas welding. Increased ferrite is produced as a byproduct of tungsten inert gas welding. Both the weld produced by tungsten inert gas welding and the starting material itself have lower ductility than the finished weld. The customized Strauss test reveals that the grain is becoming sparser and that the material is becoming less robust. The pitting corrosion resistance of shielded metal arc welding is not as high as that of welding with tungsten inert gas. When welding to tungsten inert gas, this same density of the galvanic current increases between the base metal and the weld zone. This is because the base metal and the weld zone are both made of tungsten.

Geng et al. [26], A comprehensive investigation was conducted to analyze the microstructure, microhardness, and corrosion behavior of a joint composed of 2205 duplex stainless steel. Double tungsten inert gas arc welding with filler wire was used to create the joint. There were five different regions considered in the research,

beginning with the weld metal, and ending with the base metal. The zones encompassed the region spanning from the weld metal to the base metal. Upon subjecting the weld metal from the second pass of welding to the process of reheating, it was observed that a considerable quantity of secondary austenite was present within the weld metal. Additionally, coarse ferrite grains were found to have developed in proximity to the fusion line. The remaining zones exhibited varied levels of austenite, however their microstructures closely resembled those observed in zone 1. Additionally, the study revealed that the microhardness of the material was influenced by the dispersion of alloying elements, including chromium (Cr), molybdenum (Mo), nickel (Ni), and nitrogen (N), as well as the presence of precipitates such as chromium nitride. The durability of austenite was seen to be superior to that of ferrite during the fusion line formation while the weld metal underwent melting. It was necessary to go against the flow of traffic when crossing from the fusing line to the base metal. Electrochemical testing concluded that pitting occurred more frequently in the fusion line zone and the weld metal zone than in the base metal. Furthermore, the observed surface morphologies exhibited a high degree of consistency with the findings obtained from the electrochemical experiments.

Evin, Emil & Tomá, Miroslav [27], In this paper, we examine the results of using a YLS-5000 fiber laser to weld austenitic stainless steel (AISI 304) and ferritic steel (AISI 430). The microstructure of the weld was examined using a light microscope. Tensile testing determined mechanical properties. Forging limit diagrams were generated using notched samples with radiuses of 5, 17, and 25 millimeters. Vickers hardness was used to measure the welded joint and base material. AISI 430 lost some of its malleability after being laser welded. AISI 430 weld metal has longitudinal coarse ferrite grains. Due to the coarse-grained structure of the welded connection and the continuous interface along the centerline, laser-welded AISI 430 samples failed at lower stress and strain levels than the base material. Formability was not affected by laser welding AISI 304 samples. The AISI 304 welded joint sprouted dendrites that grew in the direction of the joint's center. For uniform elongation, agreement between experimental FLD0 values and predictive equation values was better than with the strain hardening exponent. In order to determine whether or not

certain components of an exhaust system could be manufactured at a reasonable cost, hydromechanical drawings were used.

Here is Schino et al. [28], which can be found here. In this article, a comparison is made between the characteristics of carbon or, rather, stainless-clad plates. SAW overlays are used to complete the cladding process. Because of the diffusion of elements (Fe, Cr, Ni, and Mn), there is a 1.5 mm diffusion layer that forms between the stainless-steel device of cladded plates and the carbon steel device of cladded plates. This layer lowers the corrosion resistance of the device. It is possible to quantify pitting resistance by making use of the critical pitting temperature that was established by ASTM G-48 (CPT).

Michel et al. [29], The research that was conducted by C. Labesh and his colleagues [29] found that the parameters that were used to perform MIG welding had an impact on the quality of the weld as well as its efficiency and cost. The welding parameters that are utilized have an effect not only on the shape but also on the strength of a steel weld pool. Using DOE, the parameters could be fine-tuned in order to attain the desired level of quality. The DOE method investigates the variables that have an impact on the reliability and longevity of a product. In order to collect data, we will be using Taguchi experiments. In order to find the optimal welding parameters, we are going to conduct research on the characteristics of the material that is being welded. Specifically, we are going to use an orthogonal array, a signal-to-noise proportion, and an analysis of variance. The overall effect of all of these individual parameters contributes to the material's tensile strength.

Abd Razak el. at. [30], This paper examines the corrosion of welded low-carbon steel at different voltages and filler materials. Butt joint specimens were welded using the metal inert gas (MIG) technique at 19 to 21 V with 1 V intervals and ER 308L and ER 70S-6 filler materials with a 1.2 mm diameter. Welded low-carbon steel was annealed and tested for corrosion in synthetic seawater with 3.5 wt% NaCl. SEM showed microstructure changes. As welding voltage increased, welding heat input increased, reducing corrosion. Welding heat input affects corrosion rate by changing the microstructure's ferrite content. Full annealing and ER 308L filler material reduce

corrosion rates. After the corrosion test, metallography revealed iron oxides and pitting on the exposed area. Higher welding voltage, heat treatment, and ER 308L filler can reduce AISI 1010 carbon steel corrosion.

In Xie 2020 [31], The utilization of U-GTPA welding is suggested as a potential substitute for gas tungsten arc (GTA) welding. This study presents a comprehensive comparison of the microstructure, mechanical characteristics, and corrosion behavior of 316L stainless steel joints welded using the Gas Tungsten Arc (GTA) and Ultrasonic-Guided Tungsten Plasmon Arc (U-GTPA) techniques. The joint welded using U-GTPA exhibited a greater ratio of weld zone depth to breadth and a bigger area of equivalent grain zone compared to the joint welded using GTA. The utilization of U-GTPA welding technique results in a notable enhancement in both the strength and hardness of welded joints, with increases of 7.1% and 26.2% respectively, compared to joints welded using the GTA method. The grain distribution characterized by high-angle boundaries (HABs) exhibited notable variations in the U-GTPA-welded joint when subjected to pulsed arc welding. In the context of tensile tests, it was shown that the minimal proportion of the heat-affected zone (HAB) was associated with fracture in both joint specimens. Numerous high-aspect-ratio biofibers (HABs) have been shown to enhance the tensile qualities of joints. In the context of a 3.5% NaCl solution, it was shown that U-GTA WZ exhibited a lower corrosion current density and a larger corrosion potential compared to GTA WZ, despite having a higher HAB fraction. The U-GTPA WZ material exhibits a favorable corrosion rate and demonstrates notable sensitivity.

Guoliang et al. [32], Ongoing investigation is being conducted about the thermal input of dissimilar metal inert gas (MIG) welded joints. Gas Metal Arc Welding (GMAW) is a welding technology employed for the purpose of joining dissimilar materials, specifically in the case of IS2062-IS 45 C8 and IS2062-IS 103 Cr 1. The quantity of thermal energy introduced into the system has a discernible impact on the mechanical characteristics. The heat input can be influenced by factors such as voltage, current, and wire speed. This study considers two distinct input conditions. Two dissimilar joints with a low heat input are IS 2062-IS 45 C8 (3.6189 kJ/mm) and 103 Cr 1 (4.01973 kJ/mm). ii) The utilization of high-heat input dissimilar joints

is employed for the purpose of examining mechanical properties and evaluating the appropriate heat input for dissimilar joints within the existing operational conditions. The joints under consideration are IS 2062-IS 45 C8 with a specific energy absorption capacity of 3.1421 kj/mm and IS 2062-IS 103 Cr 1 with a specific energy absorption capacity of 3.70537 kj/mm.

According to Çömez 2020 [33], CMT welding is an emerging technique in arc welding that offers distinct advantages in the joining of dissimilar materials. The assessment of the corrosion characteristics shown by dissimilar aluminum joints is of utmost significance as it enables the anticipation of the probable corrosive failures resulting from welding processes. This study aims to examine the impact of heat input on the weld joints composed of AA5754-AA7075 alloys, which were welded using the Cold Metal Transfer (CMT) technique with ER5356 filler wire. The process of zinc vaporization resulted in the creation of pores within the weld metal, hence contributing to the partial melting of the AA7075 base metal. The tensile strength of both AA7075 and AA5754 base metals was seen to decrease due to excessive age, zinc evaporation, and grain coarsening. The average tensile strength of joints between AA7075 and AA5754 alloys ranges from 235 to 240 MPa. All of the samples on the AA5754 base metal side exhibited fracture. The pitting process served as the principal mechanism of corrosion. The elevated temperature resulted in an enhanced resistance to corrosion. For best corrosion resistance and strength, it is advised that the value range should fall between 95 and 110 J/mm.

Gupta et al. [34]. In addition, Huey immersion tests conducted in accordance with ASTM A262, Type C, are utilized in order to evaluate the material's resistance to corrosion damage. Hardness peaks can be found in the poorly graded high-temperature zone of the microalloyed steel. These peaks are located close to the molten interaction line (CGHAZ). No change can be observed in either the frequency or severity of hardness peaks as a result of the use of anti-stress medications or other treatments. The highest points of CGHAZ hardness are eliminated during the quenching and tempering processes (Q and T).

Saha et al. [35], A study was conducted to investigate the laser welding of nitinol sheets with a thickness of 1 millimeter. The welding process involved bead-on-plate configuration, and different levels of heat inputs were employed. The investigation focused on the geometric characteristics and microstructural properties of weld beads. The composition of the surface layer, as well as the features of corrosion and its temperature of occurrence, are influenced by the quantity of heat input. In the original sample, the elemental nickel peak was more intense relative to the background and titanium was in the Ti4+ oxidation state, as determined by X-ray photoelectron spectroscopy (XPS). The application of Auger electron spectroscopy (AES) enabled the researchers to determine that the ratio of titanium (Ti) to nickel (Ni) on the uppermost surface of the welded samples exceeded 1. This observation resulted in enhanced corrosion resistance of the samples and heightened stability of the titanium dioxide (TiO2) layer. The measured polarization resistance of the welded samples exhibited a magnitude that was tenfold more in comparison to the polarization resistance observed in the unwelded samples. The process of welding has been observed to induce alterations in the phase transformation temperatures, as evidenced by the results obtained from differential scanning calorimetry (DSC) analysis.

Huang et al. [36], The present study employed the multi-pass GTAW welding process to combine S355JR carbon steel and 316L stainless steel specimens. Characterization was performed on the dissimilar joints to evaluate their microstructure, mechanical properties, and corrosion behavior. During the welding process, the austenite and vermiform ferrite that make up the weld metal (WM) are found in a nonuniform distribution within the weld seam. X-ray diffraction investigation of the S355JR/WM interface has revealed the presence of a decarburization layer. This method of analysis, however, does not reveal any details about the M23C6 (chromium carbide) complex or any harmful phases. In the context of tensile testing, it can be observed that welded joints comprising S355JR and 316L materials consistently experience fracture within the heat-affected zone of the S355JR component. Gas Tungsten Arc Welding (GTAW) welds exhibit mechanical qualities that meet the standards set by the field of engineering. Based on the findings of electrochemical corrosion experiments, it can be concluded that WM exhibits a

comparatively lower susceptibility to corrosion when compared to 316L. In an aqueous solution with a concentration of 3.5 weight percent sodium chloride (NaCl), dissimilar welded joints composed of S355JR and 316L alloys undergo a chemical reaction resulting in the formation of iron (Fe) and iron(III) oxide-hydroxide (FeOOH).

Gan [37]. The aerospace manufacturing and transportation industries, among others, stand to benefit greatly from the emergence of the hybrid welding method known as Variable Polarity Plasma Arc-Metal Inert Gas (VPPA-MIG). The manufacture of aluminum alloy structures could benefit from this novel approach. The heat source for the hybrid welding technique is a combination of a Variable Polarity Plasma Arc (VPPA) and a Metal Inert Gas (MIG) torch. When the overall input energy of the VPPA-MIG hybrid heat source is held constant, the effect of changing the energy ratio between the VPPA arc and the MIG arc on the quality of the hybrid weld and the distribution of stress inside the hybrid welding joint is seen. Researchers used a hole-drilling method to analyze the distribution of welding residual stress in 10 mm 7A52 aluminum alloy welds as a function of the VPPA/MIG arc energy ratio. According to the results, hybrid welding's peak residual stress amplitude is positively correlated with the VPPA arc energy at which it was generated.By considering the unique characteristics of residual stress distribution during weld production, we are able to optimize the VPPA-MIG hybrid welding parameters for the 7A52 aluminum alloy. The maximum values of transverse residual stress (perpendicular to the weld) and longitudinal residual stress (parallel to the weld) are limited to 92.0 MPa and 234.3 MPa, respectively, when the VPPA arc energy ratio is set between 35% and 40%. The results show that the VPPAMIG hybrid welding technique can effectively prevent the occurrence of excessive peak magnitudes of residual stress and produce weld joints with a visually appealing macroscopic appearance when the parameters are optimized.

Lawal et al. [38]. The review was mostly about how tungsten inert gas (TIG) and metal inert gas (MIG) are used in welding. Each welding process was carefully looked at in order to understand how it works and why it's important to keep a safe, reliable weld with the right mechanical features. Also, the different uses in the

aerospace, aviation, automotive, and food packaging businesses were shown in a very important way. But the potentials and problems have been carefully looked at and recorded, especially porosity, which usually leads to hole defects at the weld joint, and plastic deformation, which is caused by the heat generated by friction. Also, the study suggested combining friction stir processes with TIG or MIG welding as an alternative way to solve the problems that come with how welded joints wear over time. So, the study could have given useful information to everyone involved, especially professional welders who need to know which way is best for welding aluminum alloys.

Subhas et al. [19], The microstructure as well as the resistance to corrosion of friction stir-welded joints made of high-nitrogen stainless steel were investigated. It was discovered that the speed of the welding had a greater influence on the amount of time that was spent welding at high temperatures than the peak temperatures themselves. In spite of the fact that nugget zones (NZs) with comparable tensile properties and hardness distributions were found in a variety of joints, pitting corrosion behavior was found to be highly variable. While joints that received a high amount of heat input pitted ferrite bands, tool wear bands were pitted by joints that received a low amount of heat input. The pitting was caused by Cr diffusion and tool wear, and extensive research was done to investigate pitting corrosion in New Zealand.

Zhang el. at. [39], Due to complex atmospheric environments, high-speed train aluminum alloy components are prone to corrosion. This will cause huge losses and reduce train stability. Cold spraying Al-based powders on damaged aluminum alloy components solved the problem. Studying microstructure, mechanical properties, and corrosion. After repair, there were a few pores and cracks. Averaging 54.5 HV, 3.4 HV, and 160.4 MPa, the restored portions are extremely strong. Cold-sprayed samples saw less mass loss than 6A01 aluminum after 1000 hours of neutral salt spray. Open-circuit potential was greater than 6A01 aluminum alloy in the patched areas. The substrate was safe because of the anode's restoration. There was less corrosion in cold-sprayed samples compared to 6A01 aluminum. Cold spray and aluminum-based powders can be used to repair high-speed train aluminum alloys.

Budiarto at el. [40]. Tests were done on the tensile strength, toughness, and microstructure of A283 Gr. C. steel with gouging welding currents. Gouging at 200 A, 300 A, and 400 A was compared to welding without gouging. SMAW is used to weld double-V joints with an angle of 600. At 300 A gouging current, the best tensile strength was 45.98 kgf/mm2, and the lowest yield was 45.51 kgf/mm2 when welding without gouging. The heat created by gouging makes the material less flexible. With a strain of 32.96%, the current 300A gouging is more likely to break than welding without gouging, which has a strain of 36.21%. When you gouge the current 400 A weld metal, you get 51 HRC, but when you join base metal without gouging, you get 33.33 HRC. Looking at the microstructure showed that adding more gouge or heat makes the grains bigger, which changes the stiffness and hardness. Based on the above test results and the current study, gouge has a big effect on the degree of hardness, bending strength, and microstructure of welding connect material A283 Gr C.

Osoba at. el. [41]. When carbon and stainless steel plates are welded together in a V-shape, the application of heat alters the shape of the weld bead as well as the microstructure and mechanical properties of the resulting weld. From the sample, eight steel plates measuring 75 mm by 30 mm by 10 mm were cut. The shielded metal arc welding technique (SMAW) at 1250 and 2030 J/mm went all the way through the plates. Even though some welds didn't have any big problems, austenite steel in particular had more weld defects than carbon steel because it had less carbon and because the width-to-depth ratio of the welder profile and the size of the produced stress were different. Carbon steel got stronger when heat was added to its heat-affected zone and fusion zone. Even though heat was added, the hardness of stainless steel was the same within the same welder zone (HAZ or FZ). The final tensile strength of stainless steel went down as heat was added, but its ductility went up. Under steady heat inputs, the amount of heat changed the shape, hardness, tensile strength, and microstructure of the weld bead in CS and SS. Heat input makes the heat-affected areas and fusion zones of weld samples made of low-carbon steel and stainless steel harder. Unlike carbon steel, heat-affected zones and fusion zones in stainless steel welds have the same hardness values no matter how much heat is added. No matter how much heat is added, stainless steel welds have better strength

characteristics than carbon steel welds. This is because the alloying content varies, and the amount of heat added affects how fast the weld area cools.

Albayati at el. [42]. Laser cladding (LC), an advanced surface modification technique employing laser technology, is frequently employed for the deposition of thin protective coatings capable of withstanding severe environmental conditions. Corrosion is responsible for approximately 50% of the instances of malfunction in oil and processing equipment. Due to the gravity of these inherent dangers, there is a pressing need to enhance the performance of oil machinery. The use of LC enhances the surface characteristics of the material, hence extending its longevity. Ti and Ni powders were deposited using the electrophoretic deposition (EPD) technique onto A283 steel alloy that had been alloyed with ND-YAG LC and surface remelted, which decreased rust failure and increased the number of life cycles. Optical microscopy, field-emission scanning electron microscopy, X-ray energy-dispersive spectrometry, atomic force microscopy, and X-ray diffraction were all used to examine the cladding sample and learn more about its microstructure, element distribution, and phase analysis. Coatings were bonded to the foundation with excellent metallurgical adhesion. Coatings were made from FeTi and FeNi, two materials with very different solidification microstructures. Mechanical properties, corrosion behavior, phase change, and structural tuning were all enhanced when LC and EPD powder were introduced to the laser mixed zone surface microstructure. Coats that have been treated with a laser melt more smoothly than untreated coats once they reach the upper surface. As an added bonus, the surface laser treatment went off without a hitch. This approach to cleaning is also safer for the environment. Pulsed laser cladding of A283 steel was analyzed for this work to determine its properties. Electrodeposition is a method used to carefully control the size and location of particles inside a single-substance layer.

Ogundimu at. el. [7]. This research looked at the effectiveness of Tungsten Inert Gas (TIG) and Metal Inert Gas (MIG) welding on type 304 austenitic metallic material. The study's goal is to find the best combination of process variables that will result in a weld joint that is flawless and has consistent levels of iron (Fe), chromium (Cr), and nickel (Ni) across all six samples. The ultimate tensile strength (UTS) in the

weld zone was measured to be 621 MPa for tungsten inert gas (TIG) welding with a current of 170 A, but for metal inert gas (MIG) welding with a current of 150 A, the UTS was found to be 568 MPa. In the context of joining type 304 austenite stainless steel, Tungsten Inert Gas (TIG) welding exhibits superior performance compared to Metal Inert Gas (MIG) welding. The welding process involved the use of MIG and TIG techniques to join six-millimeter plates composed of type 304 stainless steel in a two-pass configuration. The welds were executed with exceptional precision. The investigation focused on the examination of microstructures and mechanical properties of fused samples. The thermal output of MIG welding surpasses that of TIG welding.

In a study conducted by Alwan and Fayyadh [43], Butt weld joint pipes are commonly utilized in irrigation systems in southern Iraq, therefore this study examined how welding heat input affects the microstructure and corrosion resistance of these pipes. To do this, a V-butt junction was fabricated using AISI 1005 low-carbon steel pipes. A wide range of welding settings, including voltage, current, and heat input, were implemented. The results suggest that as the weld heat input was raised, the proportion of fusion zone (FZ) area occupied by Widmanstatten ferrite (WF), acicular ferrite (AF), and polygonal ferrite (PF) rose. It has been discovered that there is a positive correlation between the welding heat input and the corrosion current density (Icorr). This means that as the welding heat input increases, so does Icorr in weld joints. Consequently, this condition causes the rate of corrosion to increase. According to the study, when the heat input was increased to 5.151 kilojoules per millimeter, the corrosion rate reached its maximum value of 0.0757 meters per year.

According to Chao [44], MIG, commonly known as gas metal arc welding (GMAW), is a common method for combining metal workpieces. Food engineering, industrial sectors, ship construction, piping systems, storage tanks, and other fields use it. Heat input in metal inert gas welding affects butt weld joint microstructure, mechanical characteristics, and corrosion behavior. DCSP welded. The study found that weld heat input increased Widmanstatten, acicular, and polygonal ferrite in the fusion zone (FZ). However, decreased weld heat input accelerates cooling, reducing grain size.

The study found that decreasing weld heat input increased microhardness. Weld heat input also increased WM thickness and HAZ. Low-carbon steel welding heat input decreases the weld joint's impact energy in the weld metal (WM) region. Weld heat input was 2.386 KJ/mm, and impact energy was 49.17 J. Research also shows that welding current, or heat input, increases weld joint corrosion. It took 1.27 kilojoules per millimeter of welding current to raise the corrosion rate by 0.126 meters per year. The microstructure and mechanical properties of V-groove butt joints in low-carbon steel AISI 1015 were analyzed to see how welding parameters like current, speed, and plate thickness affected them. Welding heat was experimentally examined.

2.2. SUMMARY

Previous research efforts have focused on investigating the influence of various welding methods, such as MIG, TIG, MMAW, and others, on the microstructural properties of weld joints and their subsequent effects on the mechanical properties of the welded material. The study also investigated the influence of welding factors, including welding current, welding voltage, and welding speed, on the microstructure and mechanical properties of weldments. To ascertain the optimal conditions, the inquiry incorporated three experimental groups to explore the modification of welding parameters for achieving the most favorable heat input, leading to the minimal extent of the heat-affected zone (HAZ). Microstructure in the fusion zone (FZ) and heat-affected zone (HAZ), including phases and grain size, should also be studied in relation to heat input and weld parameters. Further, three specimens were tested to determine how heat input affected their corrosion behavior.

PART 3

THEORETICAL BACKGROUND

Towards the conclusion of the 19th century, a series of novel welding principles emerged, namely resistance and arc welding, which enabled the generation of sufficient electrical current. The process of electrical welding was first conducted by the utilization of carbon electrodes, a technique that was subsequently industrialized by Bemados. Subsequent to their initial utilization, steel rods were not employed thereafter. The creation and approval of a secured electrode by Oskar Kjellberg of Sweden was a significant and foundational contribution. The founding of the ESAB welding organization was influenced by the remarkable outcome of welding. In reference [45].

Experiments were done in the United States in 1940 to investigate the application of inert gases for arc shielding purposes. The feasibility of initiating an electric arc using a tungsten electrode, while preventing its melting, presents the opportunity for welding applications with or without the need of additional filler materials. The technique is commonly referred to as TIG welding, which stands for tungsten inert gas welding. Subsequently, over a span of several years, the metal inert gas welding route (MIG) was further advanced by employing a consistently provided metallic wire as an electrode. In the early stages, the gases employed for the purpose of securing were inert in nature, specifically helium or argon. POTAPEVSKI & ZARUBA made an attempt to harness CO2 due to its somewhat easier accessibility. The implementation of the "dip transfer" method effectively mitigated certain issues arising from the excessive production of spatter. Nonetheless, the procedure is often denoted as Metal Active Gas (MAG) welding when employing a moderately reactive gas such as CO2, or a gas blend like argon/CO2 [46].

There exist multiple welding techniques for the purpose of joining materials. Various techniques are employed in the construction of a wide array of buildings, encompassing medium-sized entities such as automobiles and train rolling stock, as well as bigger entities like supertankers, pipelines spanning several thousand kilometers, seaward oil stages, and offshore oil installations. Moreover, a diverse range of welding methodologies are employed in order to fabricate assemblies that may potentially obviate the necessity for welding altogether. Likewise, the application of welding is often employed in the preservation of essential infrastructures. The categorization of welding processes into two distinct groups, namely solid-state and fusion, proves to be advantageous [47]. Initially, a selection of fundamental metallic elements were joined by the fusion technique, wherein the process entailed the melting and amalgamation of these elements while consistently incorporating filler material to establish a cohesive connection that would subsequently solidify. Furthermore, it is important to note that the melting of a base metal does not occur during a solid-state process. Diffusional processes are employed as a means of establishing connections. Figure 3.1 illustrates the comprehensive range of welding procedures now employed for the purpose of joining.

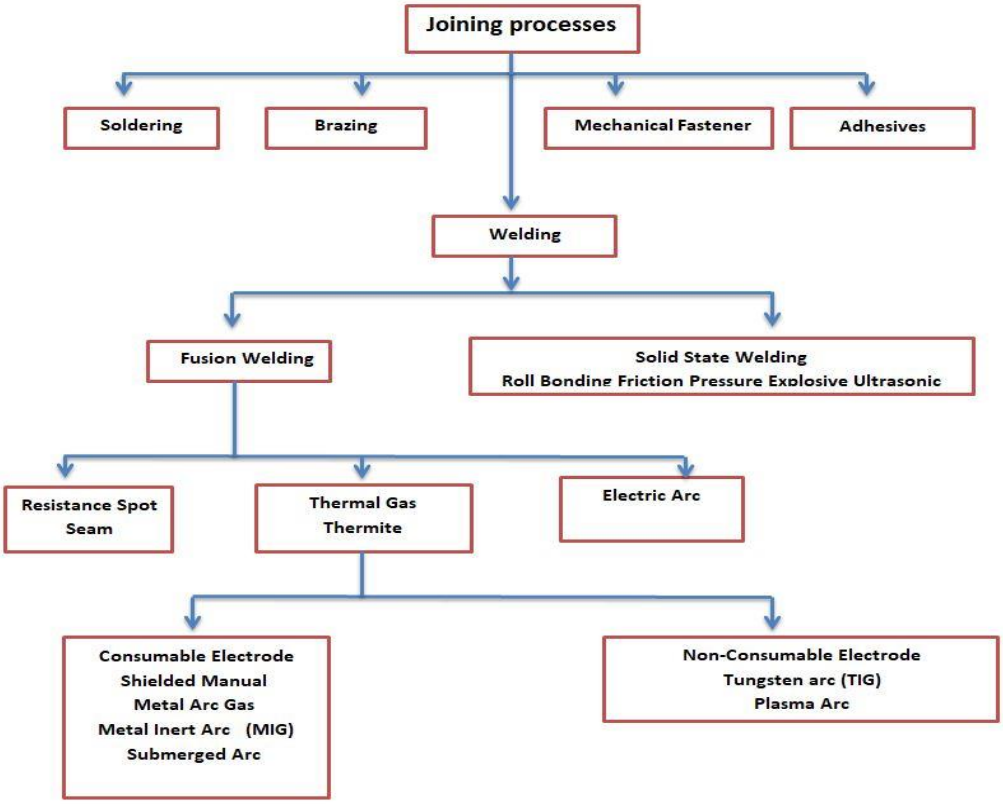

Figure 3.1. Flow charts for several Joining Process types.

3.1. ADVANTAGES AND DISADVANTAGES OF MIG WELDING

MIG welding has the following benefits [47], [48]:

1. The electrode possesses a length that is not limited, hence rendering a longer weld joint more feasible in practice.
2. The replacement of electrodes does not result in any losses in terms of stub-end or wasted labor hours.
3. The adoption of automated processes is possible.
4. In the majority of instances, the utilization of flux is unnecessary.

MIG welding has the following drawbacks [47], [48]:

1. The high expenses associated with the start-up process and ongoing maintenance.
2. The presence of stable atmospheric conditions is necessary.

3. Proficiency in high-level abilities is necessary for managing plant factors.
4. The duty cycle necessitates stringent standards, while also considering the plant.

3.2. THE ABILITY OF STEEL WELDING

Welding possesses the capability to effectively join a wide range of technical metals, albeit with certain limitations due to inadequate weldability, hence discouraging its application in certain cases. The term "weldability" is insufficiently described in relation to the evaluation of machinability. In the case of numerous engineering metals, the characteristics relevant to welding are often inadequate, resulting in a workpiece that lacks engineering utility while being united. Micro-structural modifications or fractures induced through welding processes might lead to substandard material characteristics [49]. The examination of the weldability of steel materials can be conducted using a conventional Graville diagram, as depicted in Figure 3.2. The Graville diagram is a graphical representation that illustrates the sensitivity of various steel classes to hydrogen-induced cracking, taking into account their respective carbon content and carbon equivalent (C.E.). The equation provided represents the C.E. equation (3.1).

$$C.E. = \%C + \frac{(\%Mn+\%Si)}{6} + \frac{(\%Ni+\%Cu)}{15} + \frac{(\%Cr+\%Mo+\%Si)}{5} \quad (3.1)$$

In Figure 3.2, the steels located in Zone I are characterized by their low carbon content and limited hardenability. These properties contribute to a reduced vulnerability to failure caused by hydrogen cracking during the welding process. On the other hand, Figure 3.2 illustrates that the steels classified under Zone III exhibit a combination of high carbon content and strong hardening capability, which renders them susceptible to the formation of microstructures prone to cracking during fusion welding. In Zone II, the steel exhibits higher carbon concentrations but possesses limited hardenability. In order to mitigate the hydrogen-induced cracking in these steels during welding, it is possible to regulate the cooling rate in the heat-affected zone (HAZ) by carefully managing the heat input through the implementation of preheating techniques [50].

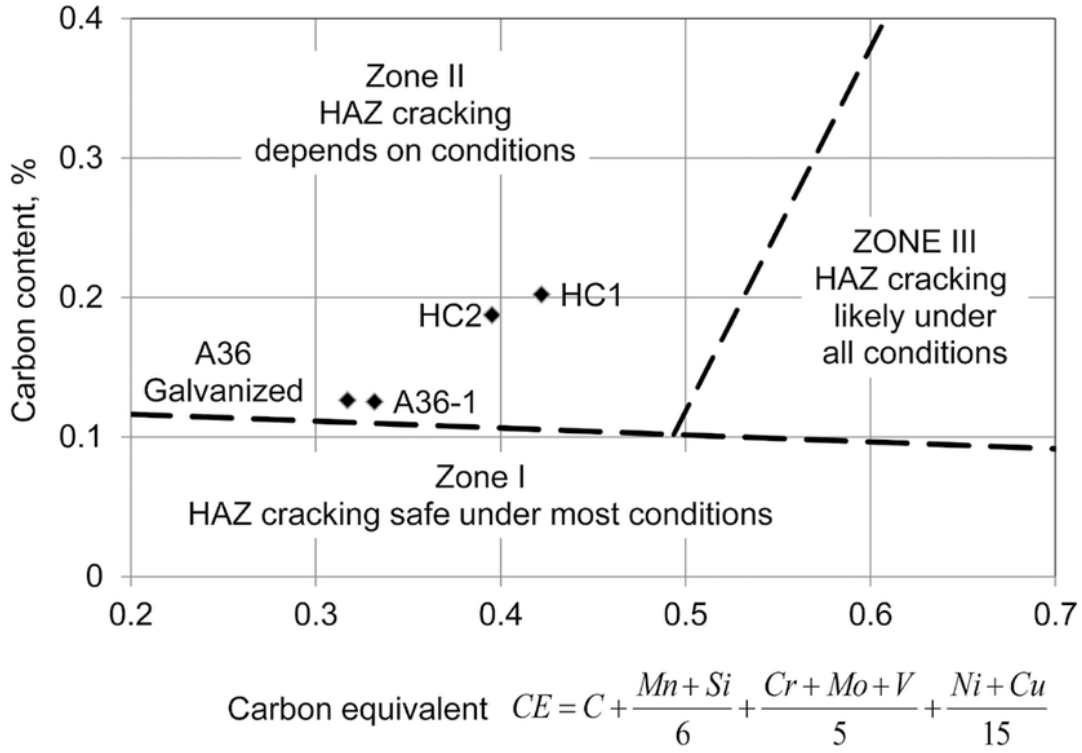

Figure 3.2. Steel Graville diagram [50].

3.3. THE WELDING OF ELECTRIC ARC

An electric arc is the discharge of electrical current between two material entities that are not in physical contact with one another. The electrode and the base metal are the two metal components used in electrical arc welding. The arc causes the gas between the electrode and the base metal to become ionized, creating plasma with temperatures greater than 10000 °C. This, in turn, affects the degree to which the base metal melts locally.

Depleting the electrode allows it to produce molten droplets within the weld joint, which can subsequently be incorporated to construct the weld zone, as proposed by this method. Because of the high temperatures present in the molten weld pool, oxidation can occur quickly during fusion welding. The generated oxides have the potential to become entrenched within the weld metal, drastically lowering the welded joint's mechanical properties and oxidation resistance. It is therefore standard practice in all electrical arc processes to guarantee that the welding pool is

appropriately shielded from the environment. This seems to be a common occurrence.

The concept of a protective gas shield is being discussed. Electric arc techniques are commonly employed in the field of engineering to combine various geometries, as exemplified in Figure 3.3. Initially, it is customary to adequately prepare the edges of the two plates that are to be linked by employing machining techniques to shape them into a V form [47], [48].

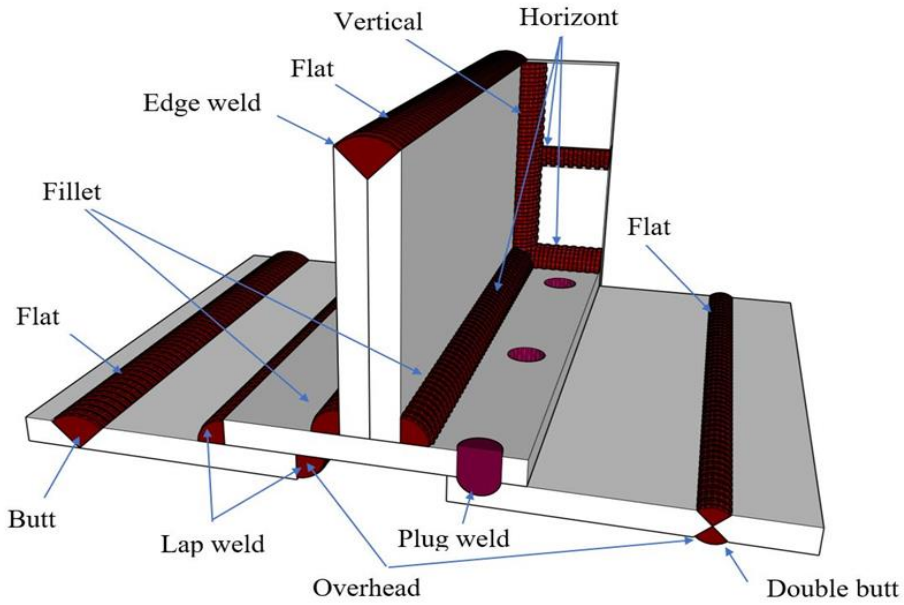

Figure 3.3. Typical shapes for electric arc welding junctions.

3.4. THE WELDING OF METAL IN AN INERT GAS ARC

It is commonly acknowledged that MIG/MAG welding is the most used technique in developed countries. A shielding gas is used in the gas metal arc welding (GMAW) process, sometimes referred to as metal inert gas welding (MIG). Depending on the type of gas used, different terms are used to describe this operation. MIG welding is the process of using an inert gas, like argon, as the shielding gas. However, it is referred to as MAG (metal active gas) welding if the gas comprises an active gas, like CO2 [51].

As shown in Figure 3.4, gas metal arc welding (GMAW) is a type of welding in which the metals to be joined are fused together by applying heat produced by an electric arc formed between a filler wire that is continually supplied and the metals to be joined. Using inert gases like argon and helium is a standard procedure to offer arc shielding and molten weld pool protection. For non-ferrous metals, in addition to alloy steels and stainless steels, argon, helium, and combinations of argon and helium are frequently used [51].

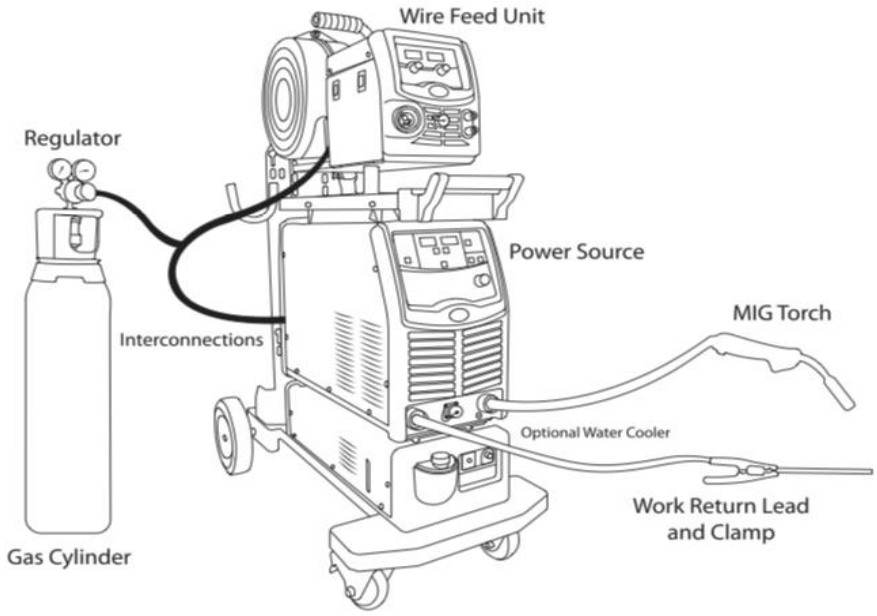

Figure 3.4. The MIG/MAG welding principle [52].

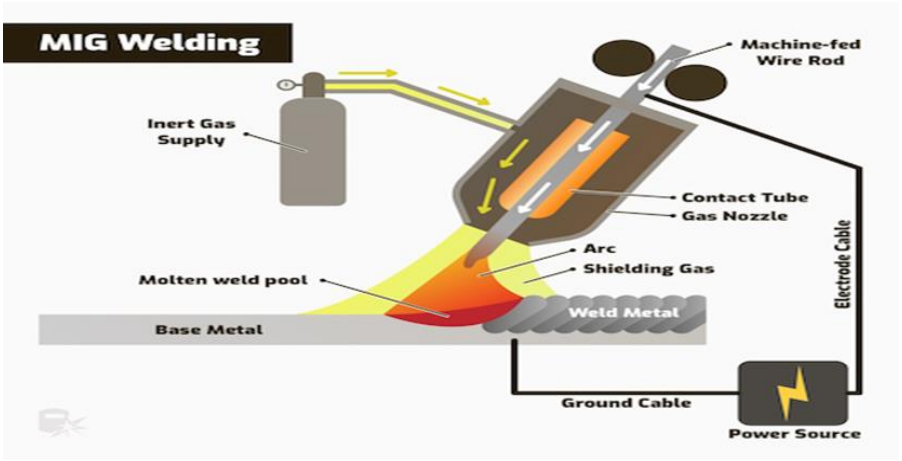

Figure 3.5. The MIG/MAG welding method [53].

3.5. WELDING PARAMETERS

The management of welding parameters is crucial for weld penetration, geometry, and overall weld quality in manual welding processes. The prudent decision regarding welding parameters increases the likelihood of producing welds that satisfy the necessary quality standards. Moreover, it is uncommon for these variables to be completely independent of each other, hence modifying one typically requires modifying several others to get the desired result.

The welder has the capability to store weld metal of superior quality and achieve welds of high caliber, provided that all relevant parameters are within the appropriate range. Once the primary metals, filler metal, and joint design have been determined, the selection of welding parameters becomes necessary. The specifics have been presented. Penetration, bead width, bead reinforcement, and deposition rate—which measures the weight of metal deposited per unit of time—are the welding parameters that most significantly affect the geometry of the weld bead [53], [54].

The MIG welding process relies on a range of welding parameters:

1. The diameter of the electrode has a significant impact on the configuration of the weld bead, hence influencing both the depth of penetration and the rate of deposition. In the context of electrochemical processes, it may be observed that when a current is applied, electrodes with smaller diameters exhibit higher current densities, resulting in increased deposition rates in comparison to electrodes with larger diameters. When encountering instances of inadequate alignment or the presence of thick plates, it is more advantageous to utilize a bigger electrode size to effectively span significant root apertures, as compared to employing a smaller electrode size.
2. The arc voltage refers to the voltage that exists between the workpiece and the electrode in the context of welding. The arc length is a determining factor for a specific electrode. The process of welding can be executed with more ease and efficiency when there is a consistent maintenance of arc voltage

variation and, consequently, the arc length. In general, it is advisable to ensure that the arc length does not exceed the diameter of the electrode.

3. The welding current is a critical factor that significantly influences various aspects of the welding process, including the velocity of melting, deposition, depth of penetration, and the extent of base metal melting. For instance, in the event that the welding current is insufficiently low, it will lead to insufficient penetration and a deficiency in
4. The rate at which electrodes are fed influences the quantity of metal that is deposited over a given length or within a specific time frame. In most of the welding equipment, the welding current is automatically regulated in conjunction with the electrode feed speed in order to ensure the maintenance of an appropriate arc length.
5. The welding speed, also known as the travel speed, refers to the linear velocity at which the arc progresses in relation to the plate along the weld joint. The velocity of welding often adheres to a specific amalgamation of welding current and arc voltage. If the welding speed exceeds a certain threshold, it may lead to reduced weld reinforcing, undercut, arc blow, porosity, and uneven bead form.
6. Electrode extension, sometimes referred to as stick out length, denotes the distance by which an electrode extends beyond the contact tip during the welding process. This particular size is generally known as "electrical stick out" and is typically of a shorter length when utilizing gas-shielded flux-cored electrodes, ranging from 3/4" to 1-1/2". The compact electrical device, characterized by a considerably elevated welding current, is capable of generating narrow, profound, and penetrating welds.
7. The selection of an appropriate shielding gas and the determination of the optimal gas flow rate are crucial considerations in various industrial processes. The selection of shielding gas is contingent upon the specific metals being worked with and has implications for various aspects of the welding process, including cost, weld temperature, arc stability, weld speed, splatter, and electrode longevity. Furthermore, it exerts an influence on other aspects of the weld material, including the depth of penetration, surface profile, porosity, corrosion resistance, strength, hardness, and brittleness.

Both Argon and Helium have been found to be effective for MIG welding applications. Pure argon is employed for welding materials that are exceptionally thin. Argon gas often facilitates an arc that exhibits enhanced smoothness and reduced noise levels.

8. The relationship between the torch and joint position. The coordination of many of these elements is essential for achieving optimal welding performance. To provide proper welding conditions, it is imperative that the working point falls within the designated working range or tolerance box for the specific welding scenario.

3.6. WELDING REGIONS

The majority of prevalent welding processes, particularly fusion welding, entail the utilization of an intensely elevated heat source to amalgamate two or more metal components. The utilization of thermal energy in the welding procedure, acknowledged as a critical factor in the creation of diverse metallic goods, has a direct impact on the mechanical and microstructural characteristics inside the welded area. Figure 3.6 illustrates the observed changes in the microstructure. The dissimilar microstructures and subsequent mechanical characteristics of the fusion zones (FZ) and heat-affected zones (HAZ) are apparent [55].

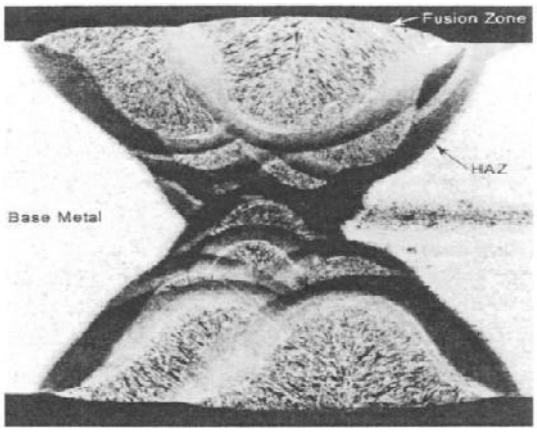

Figure 3.6. Multiple arc-welded steel plate cross-section [55].

Figure 3.7 depicts a representative cross section of a buttock joint, illustrating the sections known as the Heat Affected Zone (HAZ) and the Fusion Zone (FZ). In order

to generate the weld, a mobile heat source is employed, which moves in a direction opposed to that of the plane of the plate. Moreover, it ascertained the attributes and microstructure of each location in immediate vicinity to the welding process prior to establishing their correlation with the thermal phase of said location. The temporal variation of temperature at each discrete location is depicted in Figure 3.8.

The first point of consideration is that when point (1) is positioned immediately underneath a heat source, it undergoes a rapid increase in temperature, reaching the fusion temperature of 1540°C. The cooling rate of this region is accelerated due to the phenomenon of heat conduction, wherein thermal energy is transferred across the weld joint by means of heat propagation inside the adjacent metal. The drop-in cooling rate is observed when temperatures exceed 1540°C, which aligns with the cessation of latent heat fusion. When contrasting with point 1, it can be observed that the spots located at a greater distance from the heat source have a slower rate of cooling. Points 2, 3, and 4 exhibit temperatures surpassing the austenitization temperature threshold of 723°C within the Heat-Affected Zone (HAZ), with specific reference to steel. Point (4), situated at the periphery of the Heat Affected Zone (HAZ), exhibits a temperature above 723°C. On the other hand, point (5), situated beyond the Heat Affected Zone (HAZ), exhibits a temperature below 723°C and does not undergo austenitization [50]. Three more regions were found inside the Heat Affected Zone (HAZ) as follows: the grain growing zone, the grain refined region, and the transition region [56].

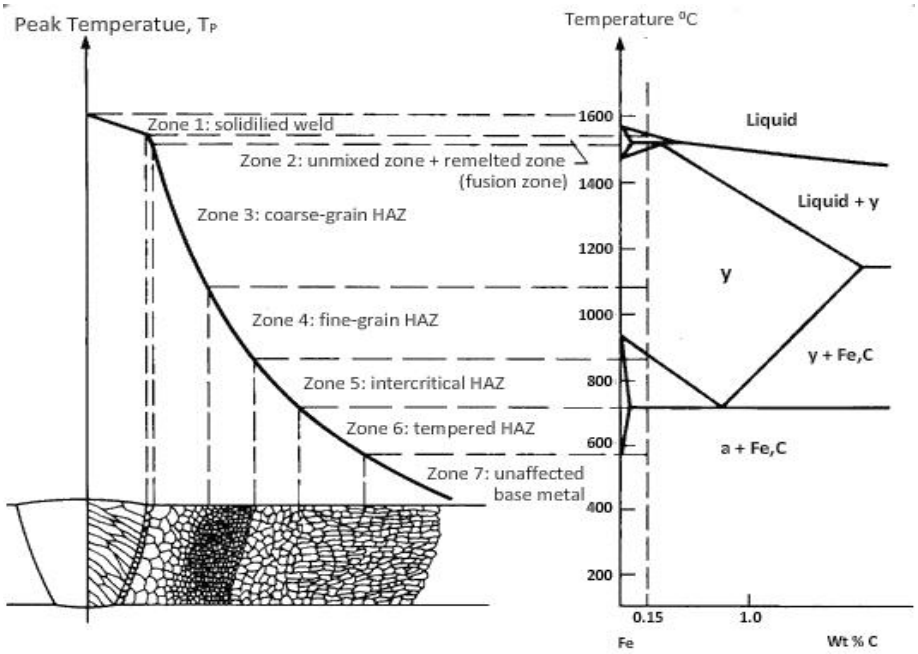

Figure 3.7. Schematic graphic showing the different WM and HAZ zones and sub-zones [29].

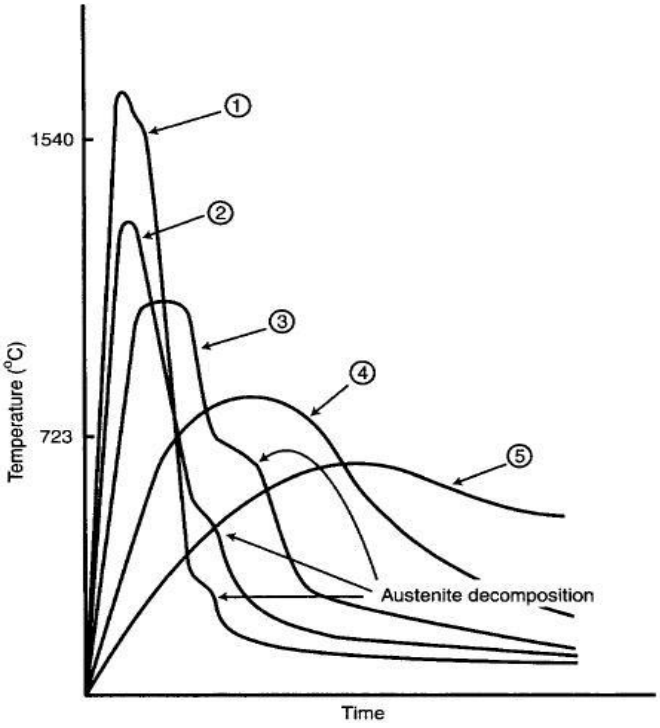

Figure 3.8. The previous picture represents a thermal cycle in welding [29].

3.7. PHASES TRANSFORMATIONS

During the cooling process in the fusion and heat-affected zones, the austenite phase experiences a significant decrease in stability below 723°C, leading to its transformation into either Martensite or a combination of α and Fe3C, depending on the rate of cooling. Points 1, 2, and 3 may undergo partial transformation into the Martensite phase due to accelerated cooling. The observed consequence of this transformation is a reduction in the rate at which cooling occurs, as depicted in Figure 3.8, which pertains to the latent heat associated with the γ Martensite transformation. In point (4), it can be observed that a significantly reduced cooling rate leads to the transformation of austenite into ferrite and cementite. The heat cycle generated during the welding process can give rise to the formation of remarkable Martensite in both the fusion and heat-affected zones [29], [56], [57].

The strength of the welded region may surpass that of the base metal due to the presence of a robust and resilient phase known as martensite. Nevertheless, this is considered unfavorable mostly because Martensite exhibits brittleness and has a minimal plastic deformation capacity. Therefore, the occurrence of stress cracking in the presence of martensitic metal can be attributed to the deformation and residual stresses resulting from the welding procedure. Hairline cracks inside the martensitic structure has the potential to precipitate premature failure of the weld joint. Although it is possible for martensite to produce either a fusion zone (FZ) or a heat-affected zone (HAZ) structure, the HAZ is generally considered to be more susceptible due to the stable chemical composition of the base material. Fillers are commonly employed in fusion welding to effectively control the chemistry of the fusion zone and mitigate the formation of martensite and its associated hardness. Fillers have a role in this region by serving as low-carbon electrodes, thereby introducing structures with low hardness.

The continuous cooling transformation (CCT) diagram is the principal method employed to assess the likelihood of Martensitic production in the hot zone of interest, commonly referred to as the heat-affected zone (HAZ). This diagram is specifically tailored for welding-related purposes. Figure 3.9 displays a

representative graph illustrating the continuous cooling transformation (CCT) for low-alloy steel. By subjecting the material to a consistent cooling process, conventional graphs depicting the correlation between time and temperature at this stage of the phase transition will exhibit a transformation into the Martensite phase, Bainite phase, or a combination of ferrite and pearlite. The CCT graph use T8/5, which represents the cooling time, as a temporal measure for welds. The temperature range exhibits variation, with values ranging from 800°C to 500°C. Currently, the prevailing norm utilized in the welding industry for assessing the rate of cooling is denoted as T8/5.

The major distinction between a welding continuous cooling transformation (CCT) map and a conventional heat-treating CCT map is in the austenitizing temperature. The region adjacent to the fusion zone, characterized by temperatures approaching the material's melting point, is the most susceptible area inside the heat-affected zone (HAZ). In traditional heat treatment methods, the temperature at which the austenitization heat treatment occurs is significantly reduced. The hardenability of steel at elevated temperatures significantly increased the probability of achieving hardened Martensite and Bainite microstructures during the welding process. Figure 3.9 depicts the complete transformation of a low alloy steel into a Martensitic structure when subjected to a cooling rate of less than 1.5 seconds from the eutectoid temperature. The formation of a composite microstructure consisting of Martensite and Bainite is achieved through a rapid cooling process lasting between 1.5 and 3.5 seconds. On the other hand, a prolonged cooling time leads to the formation of a composite microstructure including Ferrite and Pearlite. The hardness curve illustrated in Figures 3.9 showcases a range of hardness values, starting from a fully martensitic material with a hardness of 400 VPN, and extending to a material devoid of any martensite microstructure, exhibiting a hardness of 200 VPN. The hardness curve, commonly referred to as the characteristic-hardness curve (CHC), is a significant attribute of a material in the context of welding. In the majority of welded steel grades, it is typically feasible to obtain access to both the Continuous Cooling Transformation (CCT) and Continuous Heating Transformation (CHT) graphs [29].

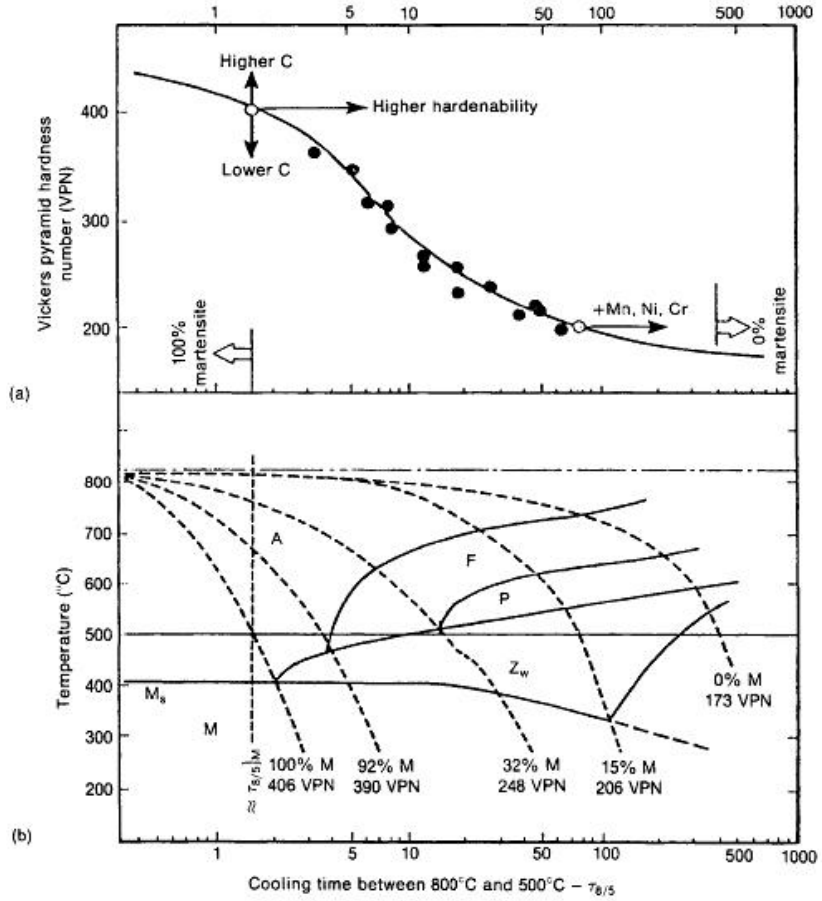

Figure 3.9. (a) The typical hardness curve and (b) A standard CCT diagram for low alloyed steel welding (0.15wt%C, 0.37wt%Si, 1.42wt%Mn [29].

3.8. HEAT INPUT

The term "heat input" refers to the thermal energy transferred during the welding process, which is facilitated by the convenience of utilizing an electric arc for most activities. The calculation involves dividing the arc voltage and current by the welding speed. Following this, electric arcs experience energy loss to the surrounding environment by radiation, heat transfer, and conduction via the gas and slag media. As a result, the efficiency of energy transmission to the welding area is less than 100% [56]. The measurement of heat input is determined using equation (3.6).

$$Q = \eta \frac{VI}{\upsilon} \tag{3.2}$$

In this context, the variables used are V to represent the welding voltage in volts, I to represent the welding current in amperes,‑to represent the weld speed in millimeters per second, and η to represent the weld transfer of heat efficiency. Table 3.2. The determination of heat input in the SI system of units involves the measurement of weld speed, expressed in millimeters per second. Furthermore, the heat input that is produced is typically quantified in joules per millimeter (J/mm) or, alternatively, when divided by 1000, in kilojoules per millimeter (kJ/mm). The typical range of heat input values in arc welding is reported to be between 0.1 and 10 kJ/mm [58].

Table 3.1. Efficiency of heat transmission in arc welding procedures [58].

process	**η**
Metal Inert Gas [MIG]	0.66-0.75
Shielded manual metal arc	0.7-0.85
Submerged Arc	0.90-0.99
Tungsten Inert Gas [TIG]	0.22-0.48

The ambient temperature history for different heat inputs is illustrated in Figure 3.13, resulting in varying cooling rates, with larger heat input leading to slower cooling and lower heat input leading to faster cooling [59]. The rate of cooling increases as temperatures decrease more rapidly, leading to many notable welding phenomena occurring during the transition of metals, such as the creation of Ferrite-Martensite steel. The high-temperature phase within weld metal, namely in the heat-affected zone (HAZ), undergoes a quenching process. The initial heat input in this scenario is referred to as the deceleration of the cooling process. The process of preheating involves the application of heat to the base metal prior to welding, resulting in a reduction in the cooling rate. Higher preheating temperatures are associated with decreased cooling rates.

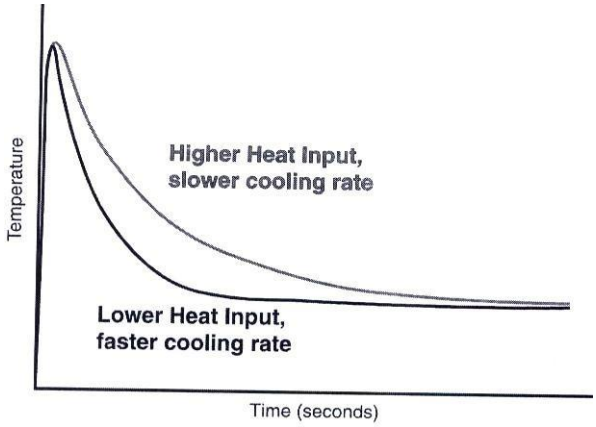

Figure 3.10. The correlation between heat intake and cooling rate [59].

PART 4

METHODOLOGY

This chapter provides a comprehensive coverage of the experimental methodologies employed in the study. The objective of this study is to investigate the heat input in the heat-affected zone (HAZ) and fusion zone (FZ) of V-groove weld butt joints welded using the metal inert gas (MIG) welding process. The heat input in welding is primarily influenced by four key factors: welding voltage, welding speed, welding current, and plate thickness. Figure 4.1 illustrates the correlation between the microstructure of the fusion zone, the heat-affected zone, and the welding parameters that govern the welding heat input.

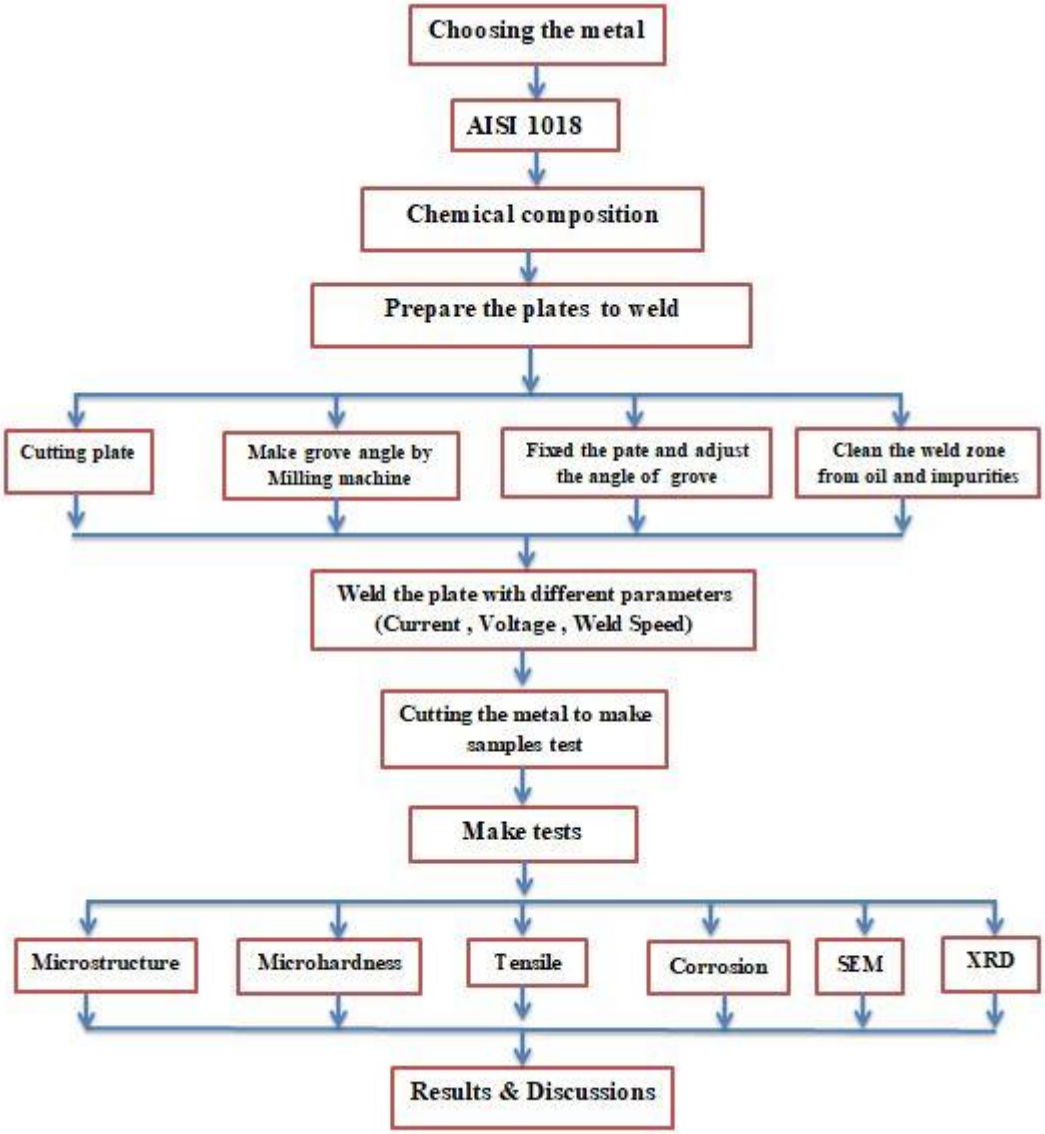

Figure 4.1. Using parameters to control the welding process.

4.1. MATERIALS

Table 4.1 displays the chemical structure of low carbon steel, more specifically known as AISI 1018. In the meanwhile, Table 4.2 presents data pertaining to the mechanical properties of the aforementioned steel variant. The first step in sample preparation entails partitioning the plate into Eight rectangular forms, with two forms designated for each sample. The specimens were appropriately prepared for the purpose of conducting various tests, including microstructure analysis, microhardness testing, corrosion assessment, scanning electron microscopy (SEM), and tensile testing. The dimensions of the specimens were measured to be 150 mm in

width, 400 mm in height, and 10 mm in thickness. The measurements are illustrated in Figure 4.2. In the microhardness tests, the samples underwent grinding using a hydraulic cutter and milling machine. This process resulted in the formation of grove welding at a temperature of 300 degrees on each side of the samples. Subsequently, two pieces of each sample were fixed together. Subsequently, the samples were subjected to welding using varying settings, leading to the emergence of samples possessing altered dimensions, namely measuring 300 mm in width, 400 mm in height, and 10 mm in thickness, as visually depicted in figure 4.3. Following this, the samples undergo a cleaning process using alcohol in order to remove any traces of oil residue prior to undergoing thermochemical treatment. In order to obtain accurate information on microstructures when observed under a microscope, the samples underwent a polishing process with a particular cloth designed for this purpose. The cloth was treated with an aluminum oxide (Al2O3) solution, characterized by a grain size of 5 m. Subsequently, the specimens underwent etching utilizing the nital solution, including a composition of 5% HNO3 and 95% alcohol. Subsequently, the specimen underwent a cleansing process with a combination of distilled water and alcohol.

Table 4.1. The low carbon steel's chemical composition.

Element	C%	Si%	Mn%	P%	S%	Cr%	Fe%	Al%
Wt.%	0.16	0.22	0.86	0.030	0.022	0.018	98.6	0.33

Table 4.2. The carbon steel's mechanical qualities (AISI 1018).

Properties	**Value**
Tensile strength, ksi [MPa]	55–75 [380–515]
Yield point, min, ksi [MPa]	30 [205]
Elongation in 8 in. [200 mm], min, %B	22
Elongation in 2 in. [50 mm], min, %B	25

The Welding wire must be compatible with the type of metal used in the manufacture of storage tanks, and for MIG welding it must be of a type (ER 70 S-6) according to AWS A5-18 [60], whose chemical and mechanical specifications are mentioned in Table 4.3.

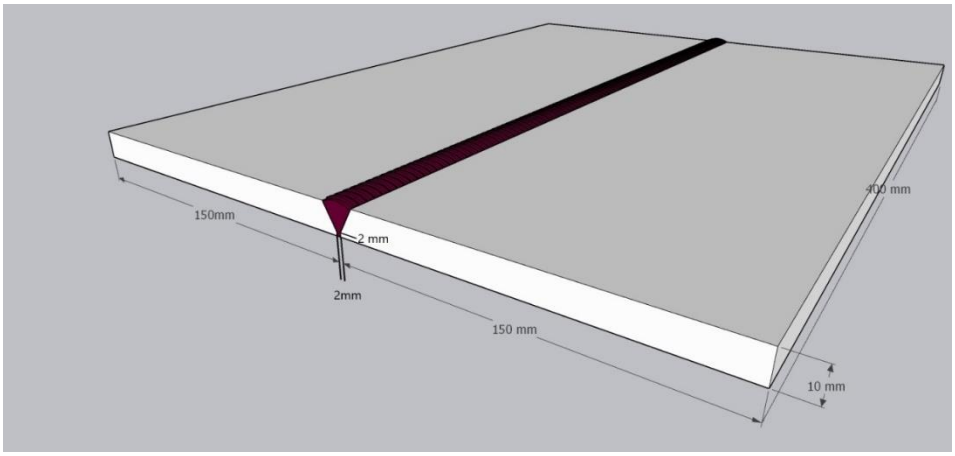

Figure 4.2. Single V-joint design of plate.

Table 4.3. Chemical and mechanical specifications of the wire welding (ER 70 S-6).

Element	**Wt.%**
C	0.07-0.15
Si	0.80-1.20
Mn	1.4
Mo	0.02
Cr	0.04
Cu	2.29
Fe	91.5
Zn	0.30
Tensile MPa	495
HB	155

4.2. EXPERIMENTAL PROCEDURE

Commence the technique of inert gas welding (MIG) subsequent to the appropriate preparation of the samples, as outlined in figure 4.3. The operation is conducted using consumable electrodes in accordance with the rules set out by the American Welding Society (AWS). The ESAB AB MIG welding machine, produced by OZAS-ESAB Ltd. in Sweden, is illustrated in figure 4.4 and was employed in this study. Additionally, it is manufactured in Poland. The process of MIG welding involves the completion of a single pass, utilizing a carbon steel electrode (ER 70 S-6) with a diameter of 1.2 mm. This particular electrode adheres to the standards set out by AWS A5.9/ASME SFA A5.9 certification. Intergranular corrosion is less prone to occur due to the low concentration of carbon. The duration of welding was recorded using a stopwatch.

Figure 4.3. Samples after prepare for welding process.

Regarding the MIG welding machine depicted in Figure 4.4, Metal Inert Gas (MIG) welding is a highly adaptable welding technique employed for the purpose of metal joining. The formation of an electric arc occurs when a consumable electrode wire and the base metal are brought into contact. Contamination is effectively prevented through the utilization of a shielding gas, often an inert gas such as argon. The essential elements are the power supply, wire feeder, welding gun, shielding gas system, and ground clamp. MIG welding is characterized by its ability to achieve high levels of productivity and versatility when working with different types of metals. Furthermore, it is considered to be a very accessible welding technique in terms of its learning curve. The user's text does not contain any information to rewrite in an academic manner.

Figure 4.4. The MIG welder used for this task.

Equations (4.1) and (4.2) employ the utilization of a specific metric to ascertain the magnitude of heat involved in welding, referred to as welding heat input. This metric also serves as a measure of the efficiency of welding heat input. The optimal range for the heat input efficiency in MIG welding is typically specified to be between 0.66 and 0.75.

$$Heat\ Input = I \times V \times \frac{0.06}{S}\left(\frac{kJ}{mm}\right) \quad (4.1)$$

$$Heat\ Input\ Efficiency = 0.75 \times (I \times V \times 0.06/S)\ (kJ/mm) \quad (4.2)$$

Q: Heat input (J/mm)
S: weld speed (mm/s)
V: welding voltage (volt)
I: welding current (Ampere)
ɳ: weld heat transfer efficiency

4.2.1. Welded Samples

Table 4.2. Welded Samples.

Pass No.	Current I	Voltage V	Travel speed mm/min	Wire Speed m/min	Time (minute)	Heat input (KJ/mm)	Heat Input Efficiency
1	178	20	185	4.5	2.16	1.155	0.808
2	170	23	240	5	1.6	0.978	0.684
3	200	24	224	6	1.78	1.286	0.900
4	227	26	380	7.5	1.05	0.932	0.652

4.2.2. Grain Size Measurements

Figure 4.5 depicts the Olympus MX-50, a metallurgical microscope commonly employed for the purpose of measuring grain size in various materials, particularly metals. The device has superior optical characteristics, offers a diverse range of illumination alternatives, and possesses the capability to establish connections with cameras to capture photos of microstructures. This technique is employed to observe and assess the sizes of grains in prepared samples. This analysis facilitates the

comprehension of material qualities and holds significant importance in domains such as quality control and research. The user did not provide any text to rewrite.

Figure 4.5. Grain Size Measurements Device.

4.2.3. Microhardness Testing

In this study, microhardness measurements were conducted to gather data regarding the mechanical characteristics of AISI 1018 low-carbon steel, including both the substrate and the hardened material. The Vickers hardness test was conducted using a digital equipment known as the Vickers hardness tester TH714, as seen in Figure 4.7. The primary components of the apparatus consist of the microscope, indent, screw, and testing table, as depicted in figure 4.6. The diamond indenter is applied to the test material in the shape of a pyramid with a square base and a top angle of 136 degrees between opposing faces, while being exposed to a load ranging from 1 to about 9 N. The complete load is typically exerted at a magnitude of 9.8 Newtons (about equivalent to 1000 grams) over a duration of 15 seconds. Three readings were obtained and the mean values were used to represent the microhardness of all the samples, as depicted in the figures. The experiments conducted at the University of Technology, specifically in the field of Production Engineering and Metallurgy. The Vickers hardness, as determined by equation (4.3) [61], is being referred to.

$$HV = \frac{1.845 * F}{D^2} \quad (4.3)$$

Where:

HV=Hardness Vickers

F= Applied load (Kg)

D^2 = Average diagonal length (mm)

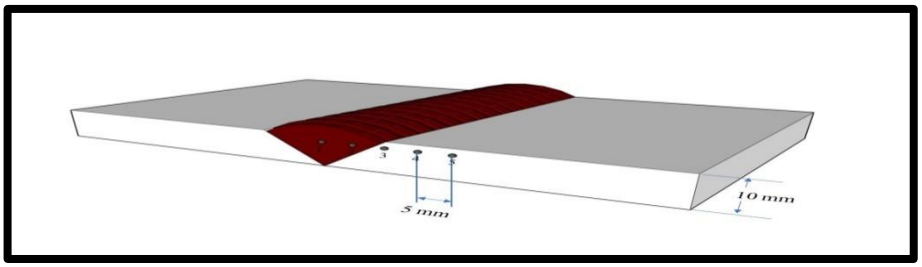

Figure 4.6. Vickers Microhardness measurements for cross section of weld sample.

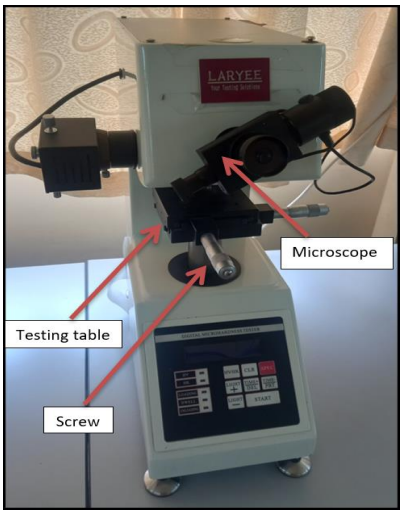

Figure 4.7. Vickers Microhardness device.

4.2.4. Tensile Test

Figure 4.8 showcases the universal testing machine, which was produced in the year 1990. This apparatus played a crucial role in the field of engineering and material science. This machine, which originated from Germany, employed controlled tension to assess material qualities until the sample experienced failure. The apparatus

included various elements such as a load cell, grips, and a crosshead. It is worth mentioning that clocks or gauge dials were employed for the manual measurement of elongation. Although these machines played a crucial role in the development of testing methods, advancements in modern technology have significantly transformed the accuracy of testing, the level of automation involved, and the process of acquiring data.

Figure 4.8. Tensile test macchine.

4.2.5. Corrosion Testing

To this end, four welded steel specimens and one base metal sample were used in a MIG welding analysis of the impact of weld heat input on weld metal corrosion properties. The specimens underwent a welding process, followed by machining to achieve a size of 1 cm^2. Subsequently, they were mechanically polished to attain a reflective surface. Following the process of being cleansed with distilled water, the specimens were subsequently stored within a desiccator for preservation. A 1.5% sodium chloride (NaCl) salt solution was employed as the electrolyte solution at a temperature of 25 °C. Polarization experiments were conducted using a standard

electro-chemical cell setup, as shown in Figure 4.9. The setup included a working electrode, an auxiliary electrode (Pt-electrode), and a Luggin/capillary for connection with a saturated calomel electrode (SCE). The experiments were performed using the "CHI 604e" Potentiostat manufactured by Chaina. Electrochemical testing was performed using a potentiostat with a scan rate of $mV.sec^{-1}$. Experiments were carried out to evaluate the polarization of weld joints in low carbon steel (AISI 1018).

Figure 4.9. Polarization cell.

In the initial stage, the potential of the steel specimen, which agreed with the calomel electrode, was assessed, and thereafter documented as a function of time. In the second phase, when the cathodic and anodic paths diverge, the polarization scan starts.

The open-circuit potential (OCP) was higher than the potential at the standard calomel electrode (SCE) reference electrode. The key results were reported in relation to the Tafel slopes measurement, as well as the corrosion potential (E_{CORR}) and current density (I_{CORR}).

It is possible to compute the rate of corrosion for uniformed corrosion using equation (4.4) [17]:

$$C.R = \frac{3.27\times10^{-3}\times i_{corr}\times W}{\rho} \quad (4.4)$$

Where,

C.R: corrosion rate (mm/year)
W: equivalent weight (grams)
ρ: density of metal or alloy (g/cm^3)
icorr: corrosion current density ($\mu A/cm^2$).

The equivalent-weight and density of carbon steel are density = 7.82 g and 7.87 g/cm^3, respectively.

4.2.6. SEM Test

In scanning electron microscopy (SEM), a material is subjected to investigation by the utilization of an electron beam, which is employed to scan and generate a magnified image. The technology, known as scanning electron microscopy (SEM) analysis and SEM microscopy, has demonstrated significant efficacy in the microanalysis and failure analysis of solid inorganic materials.

The primary purpose of a scanning electron microscope (SEM) is to generate highly magnified images by utilizing electrons instead of light for imaging. The electron beam is generated by an electron cannon located in the uppermost part of the microscope. The microscope is maintained within a vacuum environment, whereby the electron beam is directed vertically through it.

The examination and characterization of the material structure is conducted by the utilization of a scanning electron microscope, specifically the Type Axia Chemi SEM. The magnification range of Figure 4.10 is depicted, spanning from 5X to 1000000X, accompanied by resolution.

Figure 4.10. SEM device.

4.2.7. X-Ray Diffraction Analysis

The scattering of radiation in the X-ray diffraction (XRD) method is mostly attributed to the rotational motion of electrons within the atomic nucleus when X-rays interact with nanoparticles. Interference patterns arise as a consequence of the scattering of X-rays, which then undergo reflection in various directions.

Figure 4.11 depicts the X-Ray Diffraction apparatus manufactured by Panalytical Company, which is employed in the aeirs research project. The product is produced in the Netherlands.

Figure 4.11. XRD device.

PART 5

RESULTS AND DISCUSSION

This chapter presents the experimental procedures carried out on plates of low carbon steel type AISI 1018. The aforementioned steel variety was employed in the construction of the storage tank, as detailed in the experimental section. MIG welding methods were performed to join the plates together, as previously discussed. The findings presented in this chapter elucidate the impact of the welding method on the welding heat input. The alterations implemented on the microstructure yielded corresponding alterations on the mechanical properties, consequently necessitating adjustments in the welding parameters encompassing voltage, current, and speed. Furthermore, this section presents the experimental results pertaining to the final microstructure, microhardness, tensile properties, corrosion resistance, scanning electron microscopy (SEM), and X-ray diffraction (XRD) testing.

5.1. EFFECT OF HEAT INPUT ON MICROSTRUCTURE

The heat input is a critical welding parameter that significantly impacts the quality of the welded components. Variations in the quantity of heat input therefore induce alterations in the microstructure, thereby influencing the grain size. As the heat input during welding is increased, the grains within the weld pool undergo expansion; conversely, at lower heat input levels, the grains solidify at a faster rate, so impeding any further expansion of the grains. The primary factor contributing to the development of diverse ferrite microstructures is the fluctuating cooling rate experienced by the weld metal, as illustrated in Table 4-4 [62]. The microstructure of the base metal, weld metal, and heat-affected zone (HAZ) is depicted in Figure 5.1. The presented data aligns with the findings reported in reference [59].

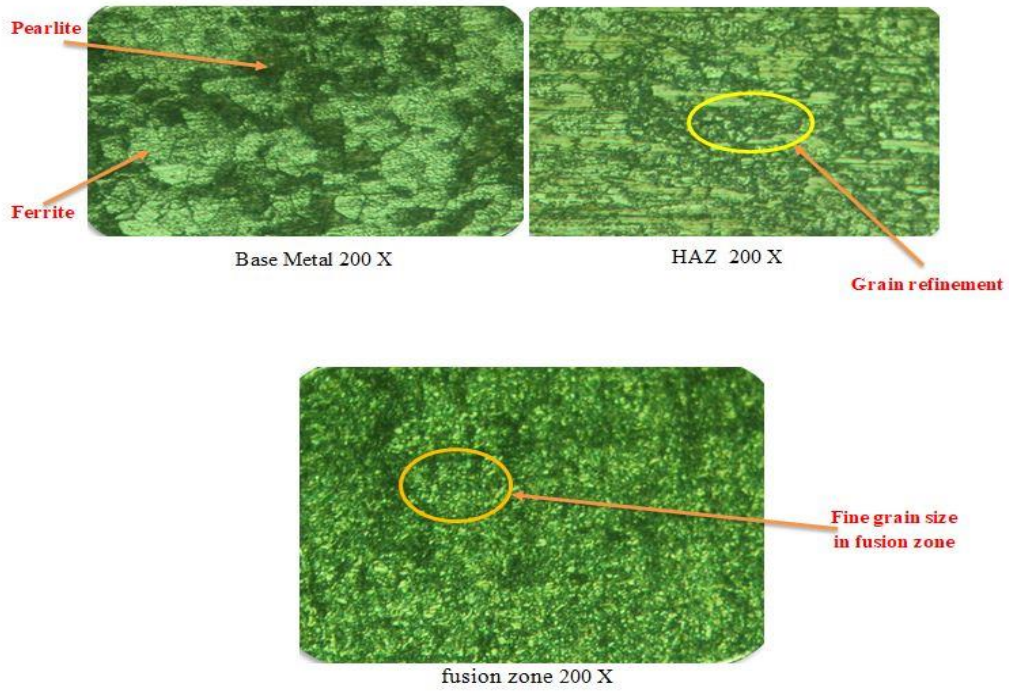

Figure 5.1. Base metal microstructure and the heat-affected zone.

Phase shifts may be observed in MIG welding as a consequence of the substantial thermal energy introduced by the welding arc. The diffusion of carbon can potentially take place due to the heating and subsequent fast cooling of the metal in the Heat Affected Zone (HAZ), resulting in a reduction in the carbon content [61]. The formation of microstructures other than pearlite can occur depending on the initial carbon concentration of the base metal and the rate of cooling. The modifications in the microstructure have the potential to impact the mechanical properties of the welded connection, hence potentially compromising its structural integrity.

The grain size within the fusion zone of MIG welding is subject to influence from multiple factors, including the composition of the base metal, heat input, cooling rate, and welding settings. This holds true for other welding processes as well. The area in which the base and filler metals undergo the process of melting and fusion in welding is commonly referred to as the fusion zone.

Welding with Metal Inert Gas (MIG) can cause significant changes to the microstructure of the fusion zone due to the introduction of thermal energy. Grain

size tends to rise with higher heat inputs and decrease with lower ones [63]. Another crucial factor is the rate of cooling; higher temperatures typically lead to coarser grain formations. Typically, a smaller grain size within the fusion zone is often favored due to several reasons:

1. Improved Mechanical Properties: Finer grain structures often result in higher strength and toughness, leading to better mechanical properties of the welded joint [18].
2. Reduced Sensitivity to Cracking: Finer grains can reduce the risk of cracking in the weld as they provide more grain boundaries that act as barriers to crack propagation [62].
3. Lower Distortion: Welds with finer grain sizes are less prone to distortion during the cooling process [63].
4. Improved Corrosion Resistance: Fine-grained structures often exhibit better resistance to corrosion and other environmental degradation [31].

5.2. EFFECT OF HEAT INPUT ON GRAIN SIZE OF WELD METAL

The impact of heat input on the microstructures, specifically the grain size, of fusion zone in the last pass (filling pass) is illustrated in Figures (5.2), (5.3), (5.4), and (5.5) using the J-Image program. The fusion zone is indicative of the highest temperature within the deposited weld metal. Typically, large grains exhibit a combination of columnar grains on one edge and ferrite and pearlite tempering grains on the other. The presence of Widmanstätten structure adjacent to the weld deposit is a possibility. Table 5.1 presents a visual representation of the relationship between temperature, namely the welding cycle, and its impact on grain size. The increase in welding current and heat input leads to an observed growth in the size of the weld metal or fusion zone. The grain growth region is located adjacent to the welded metal. Phase transitions occur within specific temperature ranges in these regions. As the base metal is approached, the macroscopic grains undergo a transition from a larger size to a smaller size. The dispersion of heat during arc welding is a crucial factor that greatly influences the mechanical characteristics of welding microstructures.

Table 5.1. results of grain size measurements.

Samples	WM (µ m)	HAZ (µ m)	BM (µ m)	Q (KJ/mm)
1	15.22	17.25	29.55	1.155
2	13.32	15.32	29.55	0.978
3	16.41	18.71	29.55	1.286
4	13.15	14.62	29.55	0.932

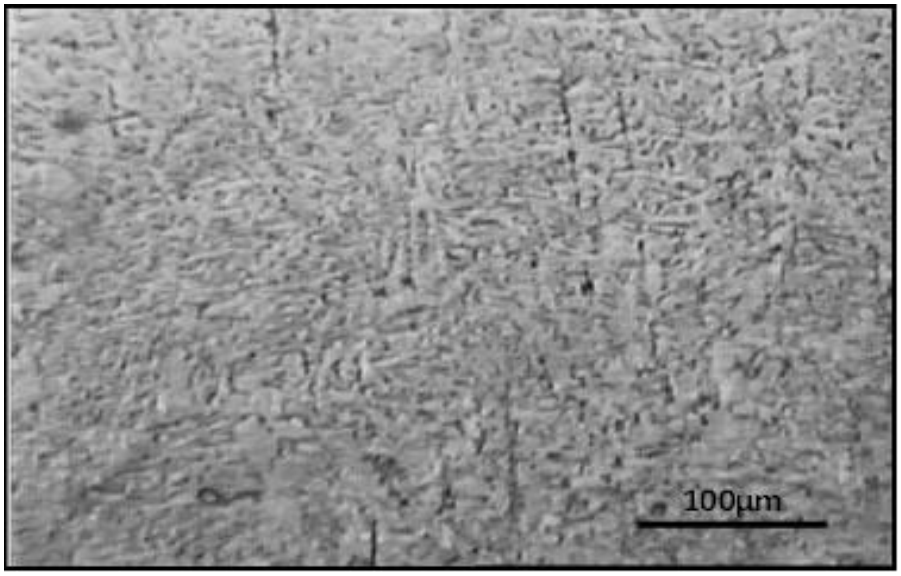

Figure 5.2. Effect of weld heat input on grain size of sample (1) when Q =1.155(KJ/mm).

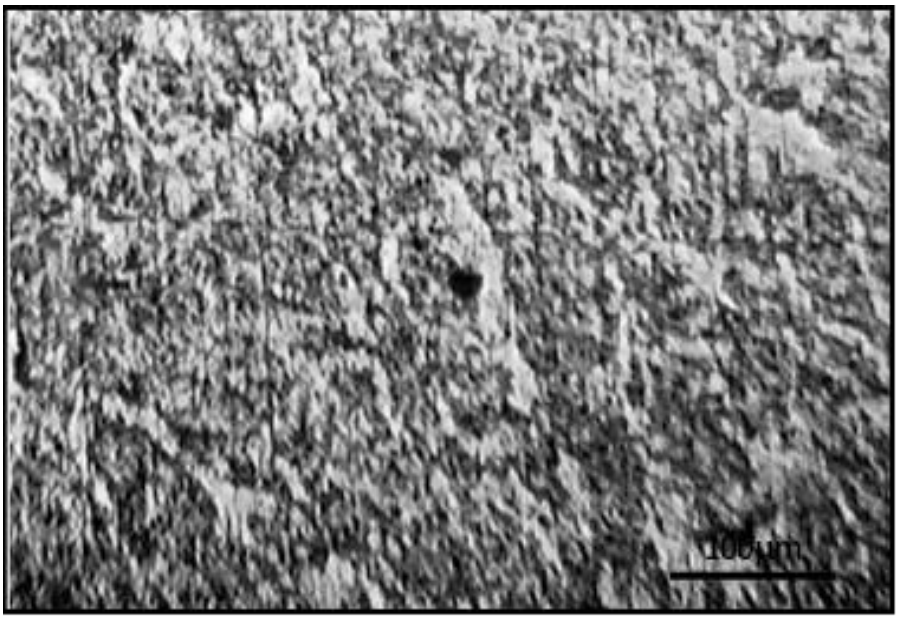

Figure 5.3. Effect of weld heat input on grain size of sample (2) when Q =0.978(KJ/mm).

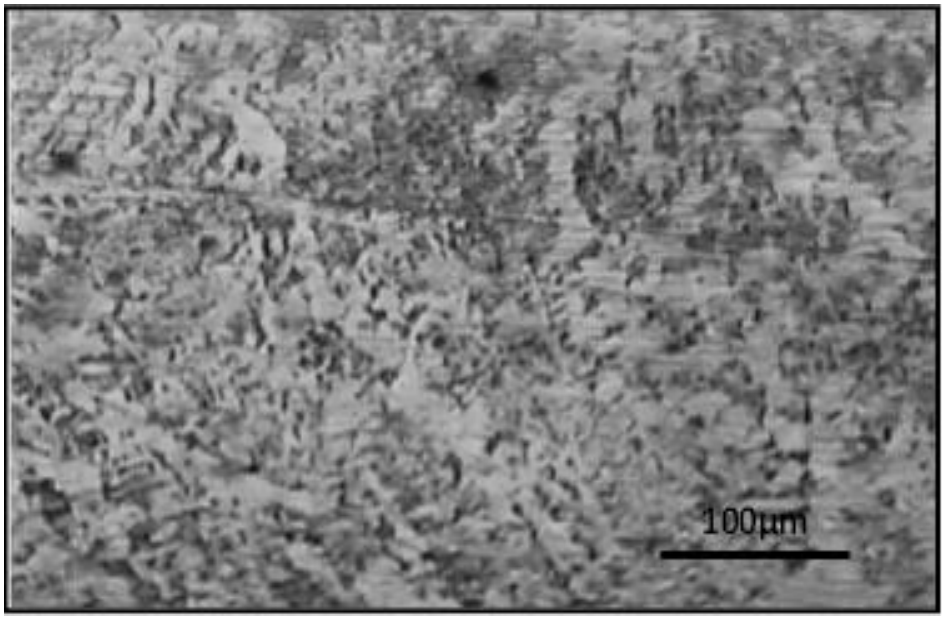

Figure 5.4. Effect of weld heat input on grain size of sample (3) when Q =1.286(KJ/mm).

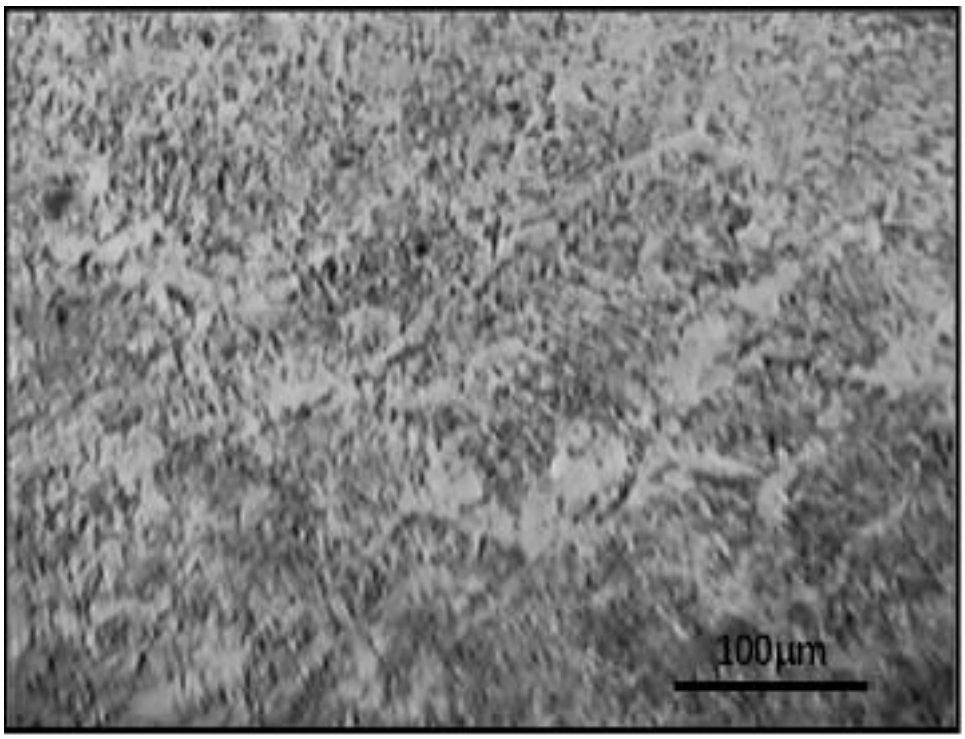

Figure 5.5. Effect of weld heat input on grain size of sample (4) when Q =0.932(KJ/mm).

5.3. EFFECT OF HEAT INPUT ON MICROHARDNESS

The microhardness test is a technique that is extensively used for analyzing the features of various weld metal zones with varied input heat for all specimens, as shown in Figure 5.6. This test may be seen in action in the microhardness test in Figure 5.6. A positive association was found between the input heat value and the degree of microhardness, as shown by the data shown in Table 5.2 and Figure 5.7. This was discovered as a result of testing for microhardness, which showed these findings. The findings of this study are in agreement with those that were described in reference [59].

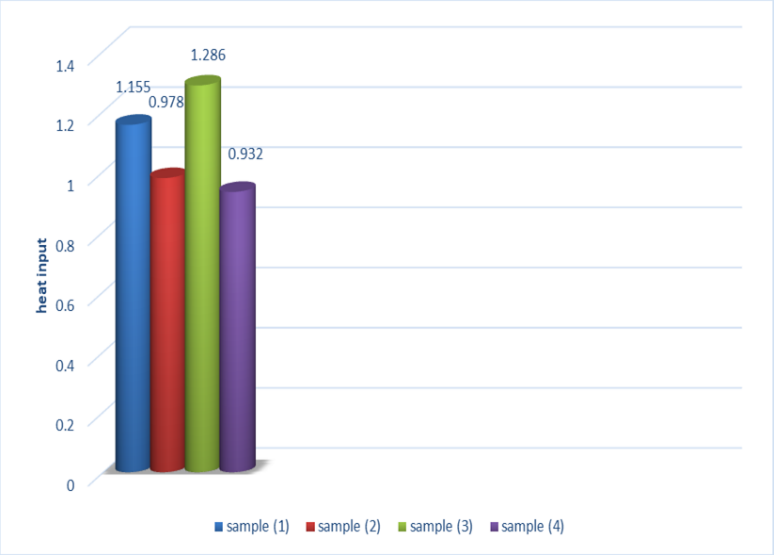

Figure 5.6. Comparison between input heat for all samples.

Table 5.2. Microhardness value for different points.

Samples No.	Microhardness Value	Q (KJ/mm)
(1)	223.1	1.155
(2)	247.4	0.978
(3)	216.6	1.286
(4)	256.96	0.932

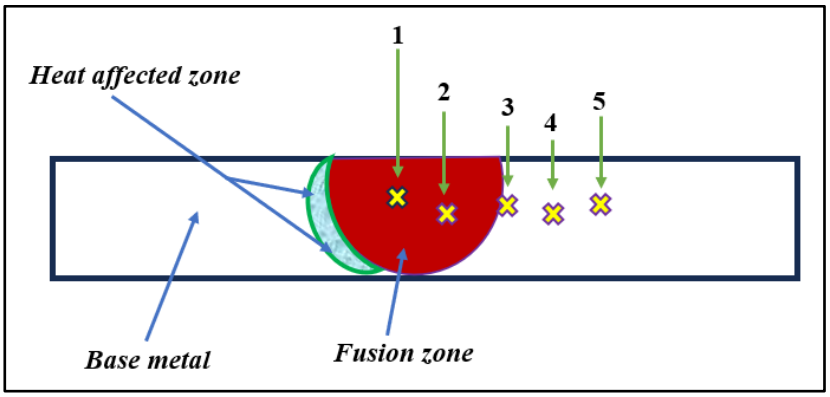

Figure 5.7. Cross section of the micro hardness points test.

The subsequent exposition provides a concise overview of the impact of heat input on the microhardness of MIG welds. The utilization of high heat input in a given process. The cooling rate of the weld pool is diminished when there is a high heat input, which can be achieved through either a high welding current or a slow welding speed. Greater grain growth can be achieved through a slower cooling process, leading to the formation of coarser microstructures. In relation to microhardness, it is commonly observed that microstructures with larger grain sizes tend to have diminished values in comparison to microstructures with finer grain sizes. minimal thermal energy input In contrast, increased welding speeds or reduced welding currents result in accelerated cooling rates, hence yielding more refined microstructures. Finer microstructures generally exhibit higher microhardness [64].

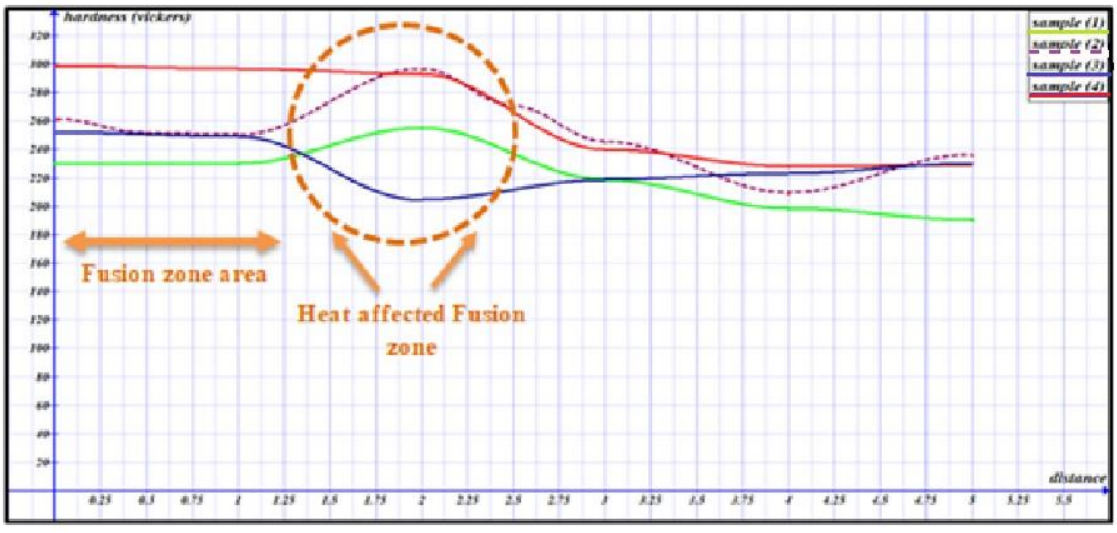

Figure 5.8. Hardness results for all samples.

Figure (5.8) shown the results that increased heat input during the welding process caused an decrease in hardness value, as seen in sample (3), but decreasing the value of heat can result in increased hardness as seen in sample (4) . This is related to the change accrued in microstructure, which was discussed in the previous section.

5.4. EFFECT OF WELD HEAT INPUT IN TENSILE TEST.

The tensile test is a standard method used to evaluate the mechanical properties of materials such as (yield point, ultimate stress, fracture stress and displacement) in weld joint as shown in Table 5.3. When it comes to MIG, the tensile test is an important way to assess the strength and ductility of the welded joint as shown in Figure 5.10. Tensile strength is also a critical mechanical property that measures the resistance of a material to being tensile test on apart or stretched [65].

The welding speed at which the welder moves the welding torch along the joint affects the cooling rate of the weld pool and the overall heat input. Proper control of travel speed is essential to achieving a balanced and consistent weld bead, which contributes to good tensile strength. Also, welding speed is one of the critical process parameters that can influence the welding quality, including the tensile strength.

Table 5.3. Tensile strength results for all specimens.

Samples	Yield stress Mpa	Ultimate tensile stress Mpa	Q (KJ/mm)
(1)	422.42	543.5	1.155
(2)	431.78	565.25	0.978
(3)	419.13	541.55	1.286
(4)	445.78	598.9	0.932

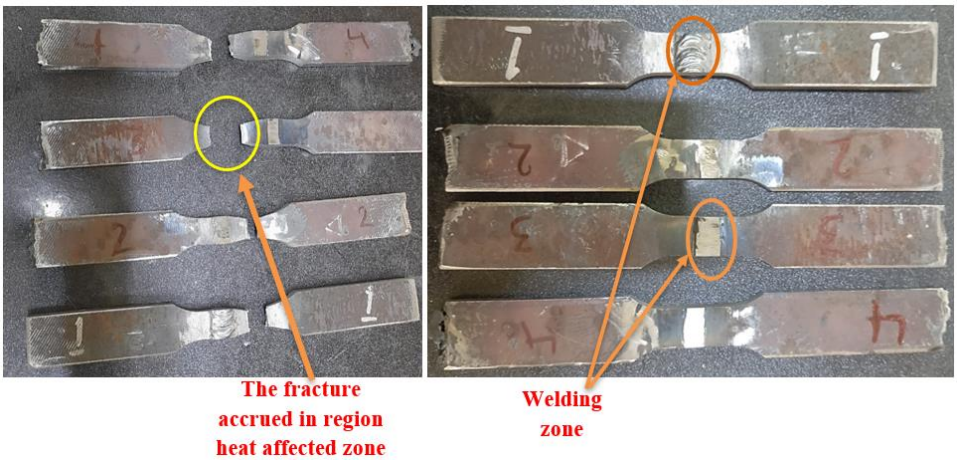

Figure 5.9. Tensile specimens, before and after the tensile test.

The heating process in MIG welding can induce a temperature gradient, potentially leading to modifications in the microstructure of the metals. The heat-affected zone (HAZ) is subject to a variety of temperatures, with the highest thermal energy being imparted in proximity to the weld and gradually diminishing as the distance from the weld increases. The process of grain growth is a significant factor contributing to the increased brittleness of the Heat Affected Zone (HAZ). The rate of cooling in welding is inversely proportional to the heat input, such that a lower heat input will facilitate a more rapid cooling process, leading to a reduced size of the heat-affected zone (HAZ). Conversely, a higher heat input will induce a slower cooling rate, thereby causing an enlargement of the HAZ inside the identical material. Moreover, as the welding process decelerates, the size of the Heat Affected Zone (HAZ) also expands. The cooling process experienced by the metal in the Heat Affected Zone (HAZ) might lead to the formation of larger and more coarse grains. As illustrated in Figure 5.9, the presence of bigger grains might act as locations of stress concentration, so augmenting the material's vulnerability to the initiation and propagation of cracks, ultimately leading to the failure of the welding procedure. Within the context of the Hazardous Area Zone (HAZ), the presence of residual stress has the potential to initiate and propagate cracks, provided that it exceeds the material's strength. The fracture in the previous incident occurred within the HAZ region [62].

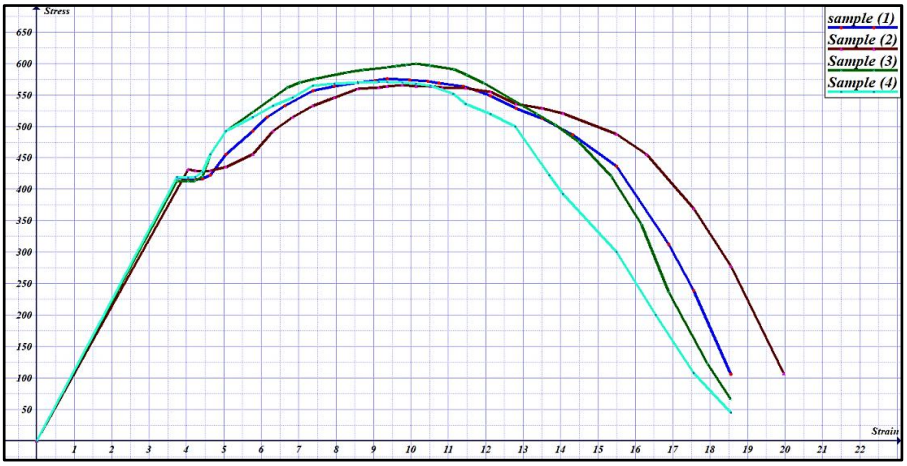

Figure 5.10. Tensile test results for all specimens.

As shown in the results, increasing heat input during the welding process can cause an increase in the size of fusion zone, so higher heat input can lead to better fusion between the weld metal and the base metal. This improved fusion can enhance the strength of the joint; also, more heat added causes increased penetration, which can result in deeper penetration into the base material. This state creates a stiffer weld with improved mechanical properties.

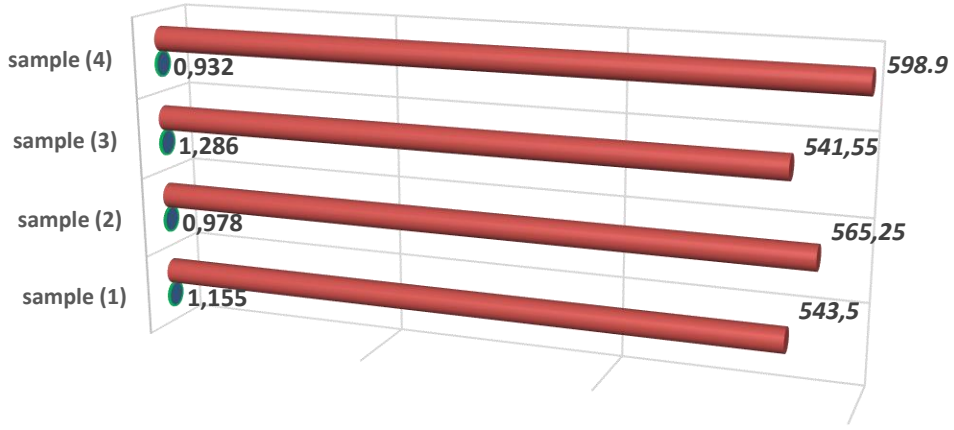

	sample (1)	sample (2)	sample (3)	sample (4)
tensile strength	543,5	565,25	541,55	598,9
heat input	1,155	0,978	1,286	0,932

Figure 5.11. Relation between tensile strength and input heat during welding process.

High heat input typically leads to increased energy transmission to the weld surface and a broader weld pool. Slower rates of cooling can be attributed to the

phenomenon wherein the additional heat is dispersed throughout a larger volume of material. The potential consequence of this phenomenon is the alteration of the microstructure of the weld, resulting in an increase in grain sizes. This, in turn, may influence the mechanical properties of the welded joint, namely its tensile strength.

5.5. EFFECT OF WELD HEAT INPUT ON CORROSION RESISTANCE

Corrosion refers to the chemical or electrochemical process wherein metal components and their alloys sustain damage as a consequence of their interaction with the surrounding environment, particularly when exposed to corrosive agents such as salt or other mediums.

The resistance to corrosion of a welded joint may be influenced by the heat input during the MIG welding process, which can affect the microstructure, residual stresses, and chemical composition of the junction. In order to maintain the desired corrosion performance of MIG-welded components, it is imperative to exercise meticulous control over welding circumstances and material selection [66].

Table 5.4. Corrosion rate of fusion zone and base metal.

ITEM	E corr. (volt)	I corr. (Amp.)	Corr. Rate mm/year	Q (KJ/mm)
Base metal	-0.723	3.596×10^{-5}	0.419	-------
1	-0.306	8.013×10^{-6}	0.093	1.155
2	-0.851	5.656×10^{-5}	0.659	0.978
3	-0.389	3.302×10^{-6}	0.038	1.286
4	-0.549	8.774×10^{-4}	0.237	0.932

Table 5.5. Corrosion rate in HAZ.

ITEM	E corr. (volt)	I corr. (Amp.)	Corr. Rate mm/year	Q (KJ/mm)
1	-0.942	5.286×10^{-5}	0.616	1.155
2	-0.964	1.352×10^{-4}	1.577	0.978
3	-0.763	1.904×10^{-5}	0.222	1.286
4	-0.944	4.017×10^{-4}	2.847	0.932

The corrosion test findings suggest that the rate of corrosion for the base metal will be 0.419 due to the absence of thermal stress from welding in the fusion zone, as depicted in Figure 5.12. This can be attributed to the fact that both the base metal and the fusion zone consist of the same metal. The aforementioned value is commonly recognized as the principal criterion for comparing corrosion values.

It is seen that the sample No. 3 exhibits the lowest corrosion current (I_{corr}) and corrosion rate when subjected to the highest heat input. This can be attributed to the fact that the sample possesses the highest magnitude in tensile strength. The determination is made by conducting a comparative analysis between the heat input values and the corrosion test outcomes of the fusion zone, as presented in table 5.4, and the heat impacted zone, as displayed in table 5.5. Figure 5.13 presents a comparison of the corrosion rates between the fusion zone and the heat-affected zone. It is observed that sample No. 3 exhibits the lowest corrosion rate value.

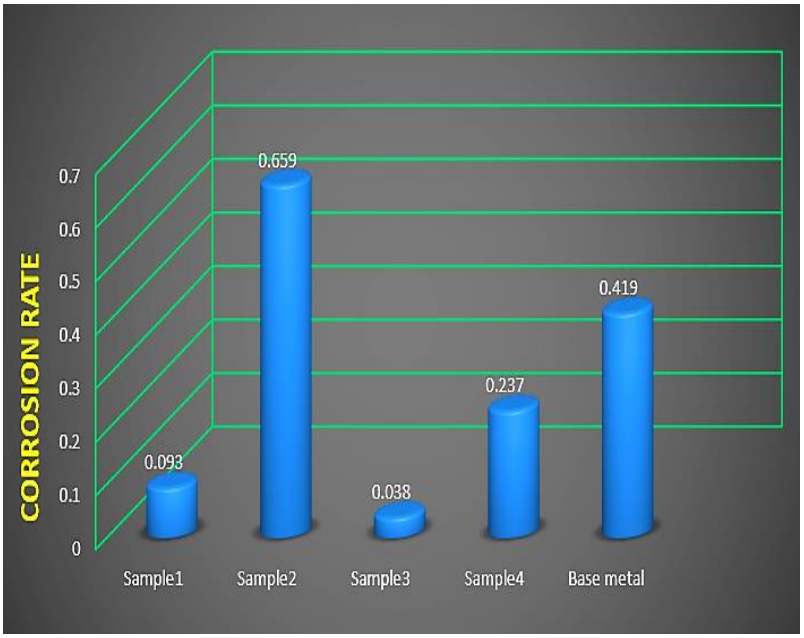

Figure 5.12. Corrosion rate for base metal and fusion zone.

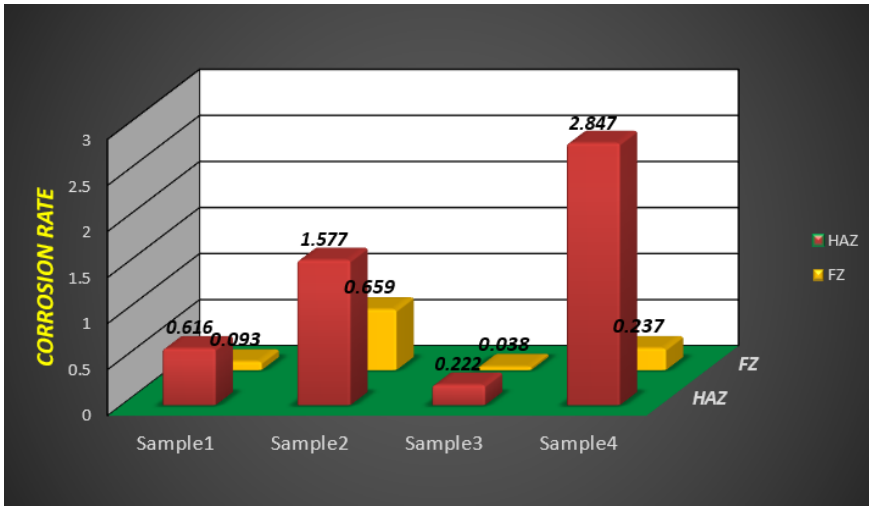

Figure 5.13. Comparison Corrosion rate for heat affected zone and fusion zone.

In Figures 5.14 and 5.15 provide an elucidation of the influence of corrosion current on corrosion resistance in the fusion zone and heat affected zone, respectively. These figures demonstrate that an escalation in corrosion current results in a decline in corrosion resistance.

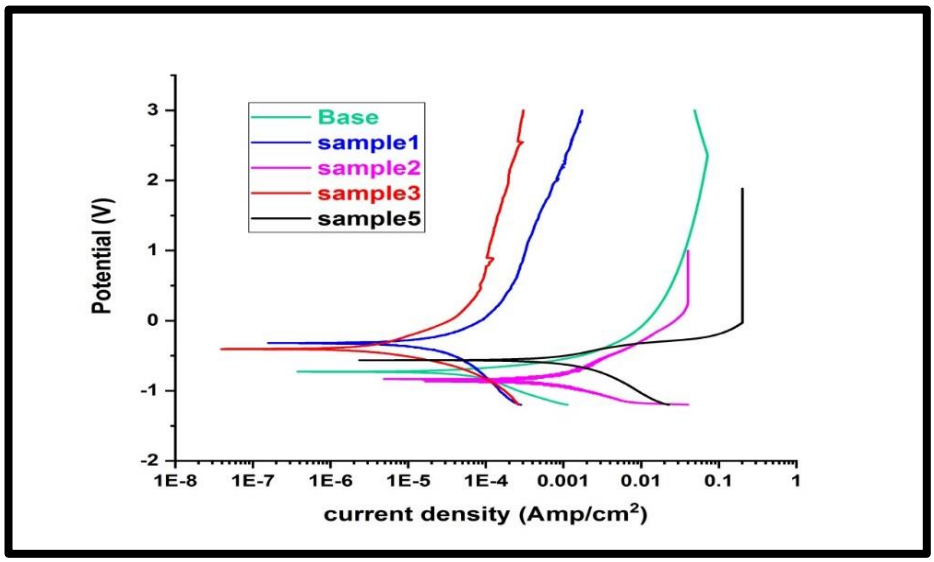

Figure 5.14. Polarization waves of (FZ and BM) in (1.5% NaCl).

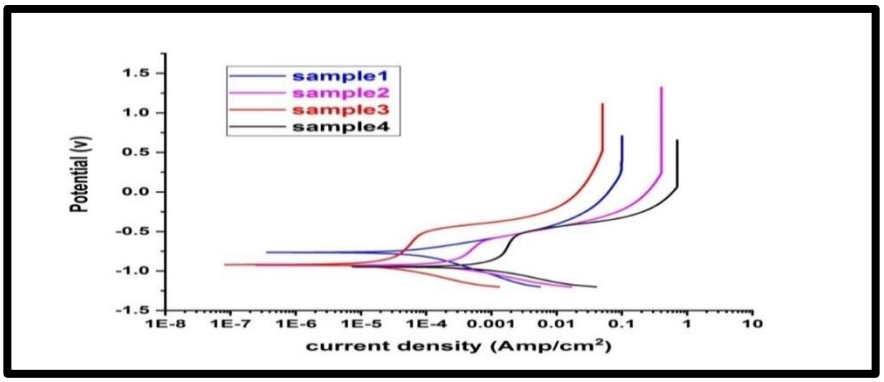

Figure 5.15. Polarization waves of (HAZ) in (1.5% NaCl).

5.6. SEM RESULT

SEM (Scan Electron Microscopy) denoted the topography surface of weldment zones as WM, HAZ and BM with different heat input. Figure 5-16. was shown the surface topography of welded metal, also appeared the surface topography of WM and denoted the flow metal in welded metal.

Increasing the weld heat input in samples resulting from changing in weld parameter gives rise to emersion welding defect.

Figure 5-17 shown the welding defect in WM resulting from increasing the (heat input) respectively, in low heat input the weld defect was *"spattering"* in different regions, with an enhancement the heat input will be configured a small *"vacancy"* another type of weld defect. Highest heat input leading to made *"largest vacancy"* and the formation of some *"microscopic cracks"*.

The scanning electron microscope (SEM) test provided a visual narrative of the topographic intricacies within the welded zones. This visual analysis further supplemented the conclusions drawn from other tests, offering a comprehensive understanding of the effects of varying welding parameters on the structure of the weld joint.

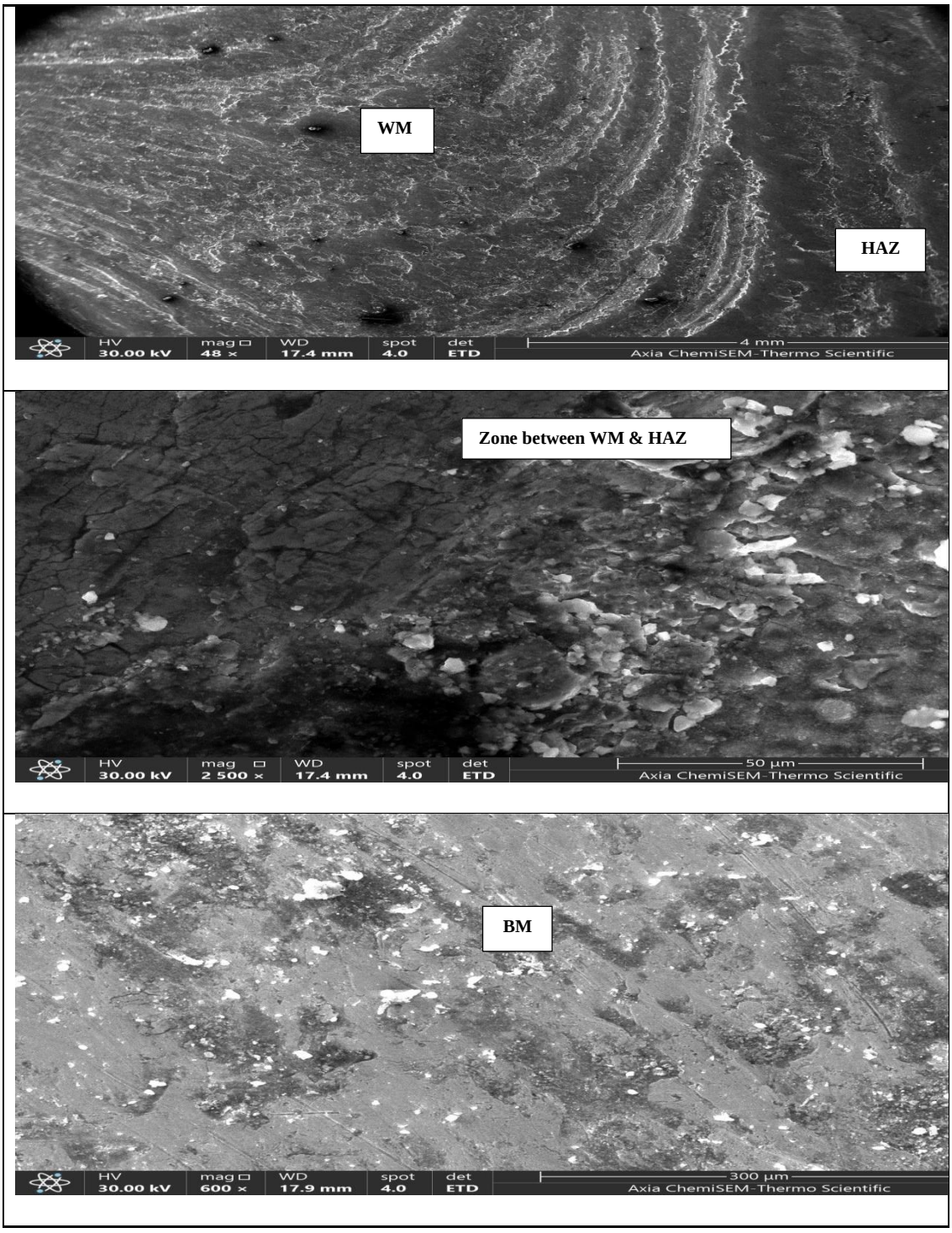

Figure 5.16. SEM Test For WM, HAZ and BM.

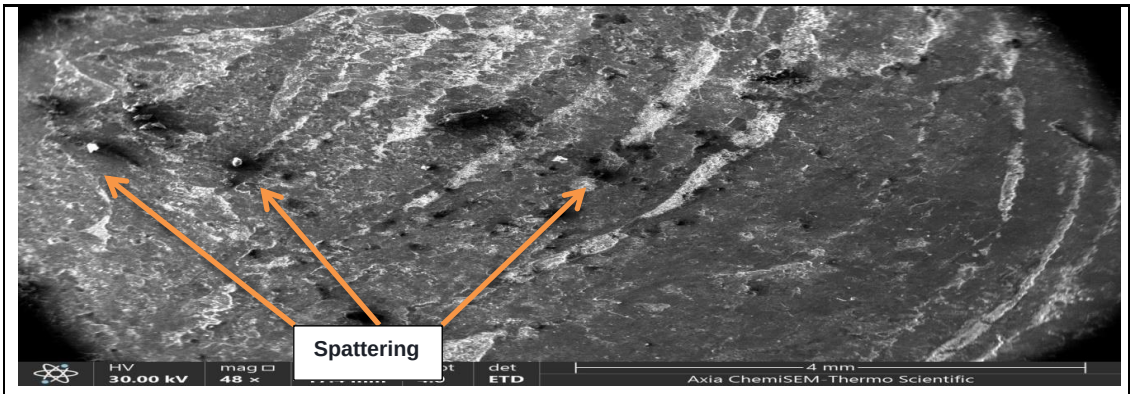

Weld defect for (low heat input)

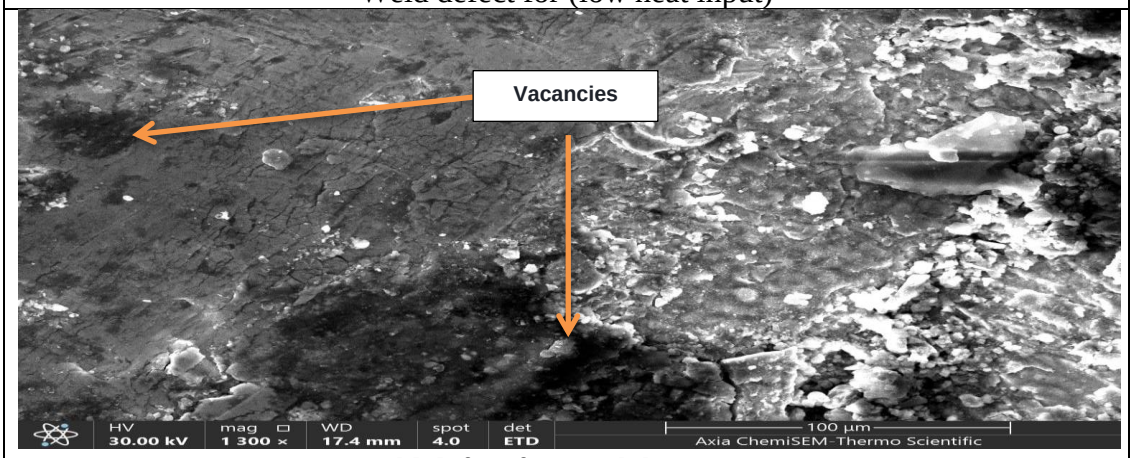

Weld defect for (High heat input)

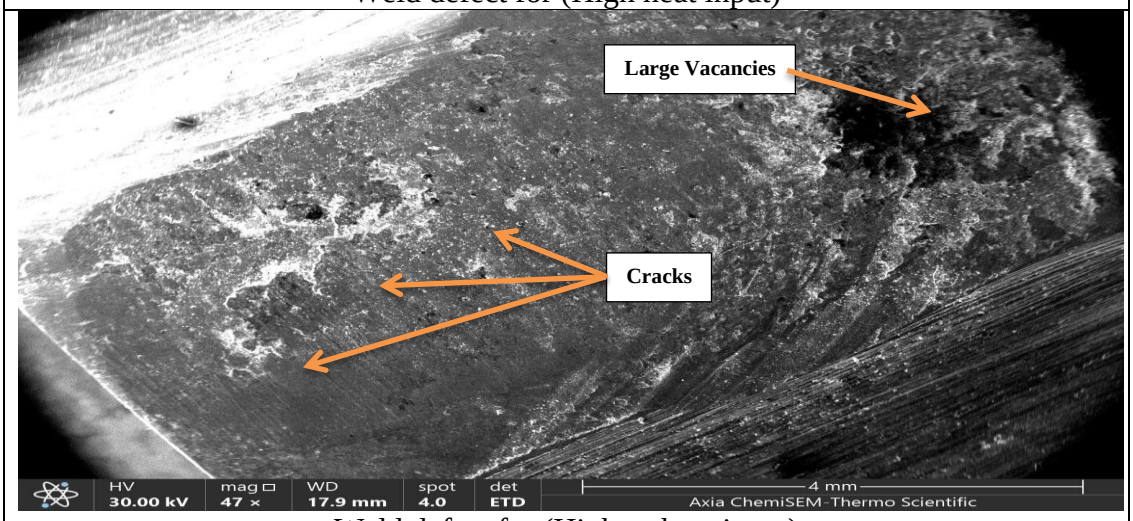

Weld defect for (Highest heat input)

Figure 5.17. Weld Defect in WM by increasing the heat input respective.

5.7. XRD RESULTE

X-ray diffraction was utilized in order to investigate the phases that manifested themselves as a result of the phase transition that took place in the weld metal joints

as a consequence of the high temperatures that were caused by the various heat inputs and the subsequent cooling.

The sample is made up of plain carbon steel, which is a type of low-carbon steel. The microstructure of this steel consists of ferrite, which is predominantly composed of iron, as well as perlite, which is a composite phase consisting of cementite and ferrite. Even if they are only found in extremely minute quantities, the alloying elements and impurities that are present in the filler metal are not likely to be detected by the X-ray diffraction (XRD) investigation. The X-ray diffraction (XRD) examination is going to look for the pure iron phase and the cementite phase, both of which have been detected before. These are the phases that are predicted to be found.

In Table 5-5 and Figures 5.18, the phase change phenomenon is elucidated in relation to several weld parameters, specifically the heat input which is influenced by weld current, voltage, and weld speed. The process of carbide (Fe_3C) cementite and pure iron (Fe) phase production. The phase transformation in the weldment of sample 2 is elucidated in Figure 5.19 and table 5-5, which highlight the occurrence of carbide production (Fe_3C) and the presence of iron. The phase transformation in sample 3, as observed in Figure 5-20, reveals the presence of carbide phases (Fe_3C) and (Fe_2C). It is noteworthy that an increase in weld heat input has an influence on the creation of carbides, as indicated in Table 5-5. In Figure 5-20, the creation of carbide (Fe_3C) and its association with iron is elucidated, in accordance with the information provided in Table 5-5.

Table 5.6. X-ray diffraction result.

Sample No.	**Pos. [°2θ]**	**d-spacing [Å]**	**d-standard [Å]**	**Phases**	**Q (KJ/mm)**
1	45.5285 82.8421	1.99074 1.164	2.02 1.44	Fe_3C ℰ-Fe	1.155
2	45.159 65.545	1.982 1.423	2.00 1.423	Fe_3C ℰ-Fe	0.978
3	45.520 82.981	1.990 1.162	2.02 1.44	Fe_3C Fe_2C	1.286
4	44.761 82.545	1.990 1.162	2.02 1.44	Fe_3C ℰ-Fe	0.932

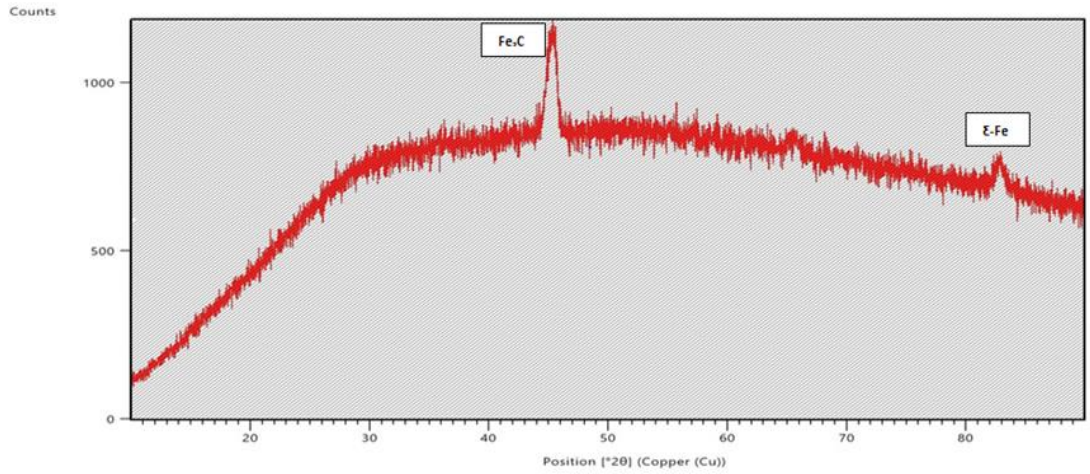

Figure 5.18. XRD results for sample (1) when Q =1.155(KJ/mm)

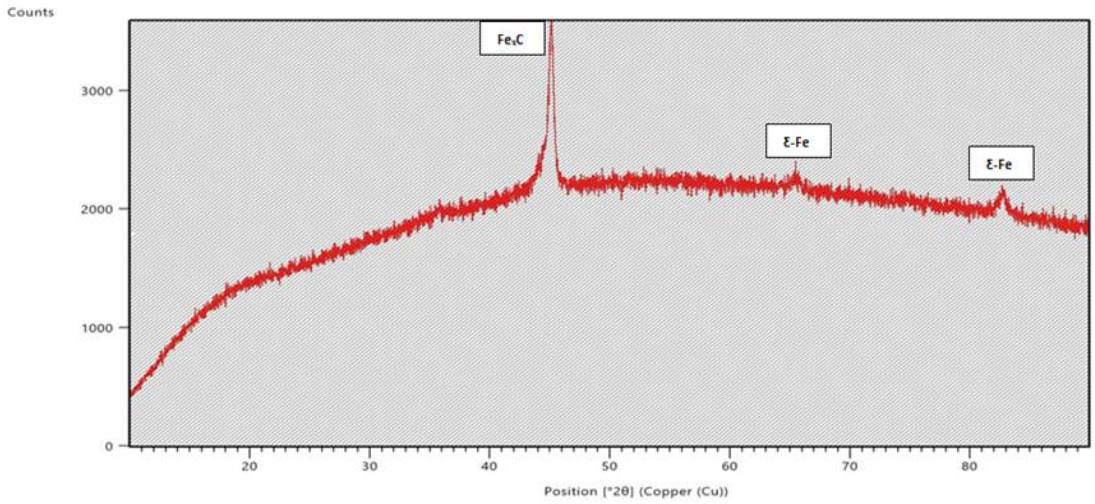

Figure 5.19. XRD results for sample (2) when Q =0.978(KJ/mm).

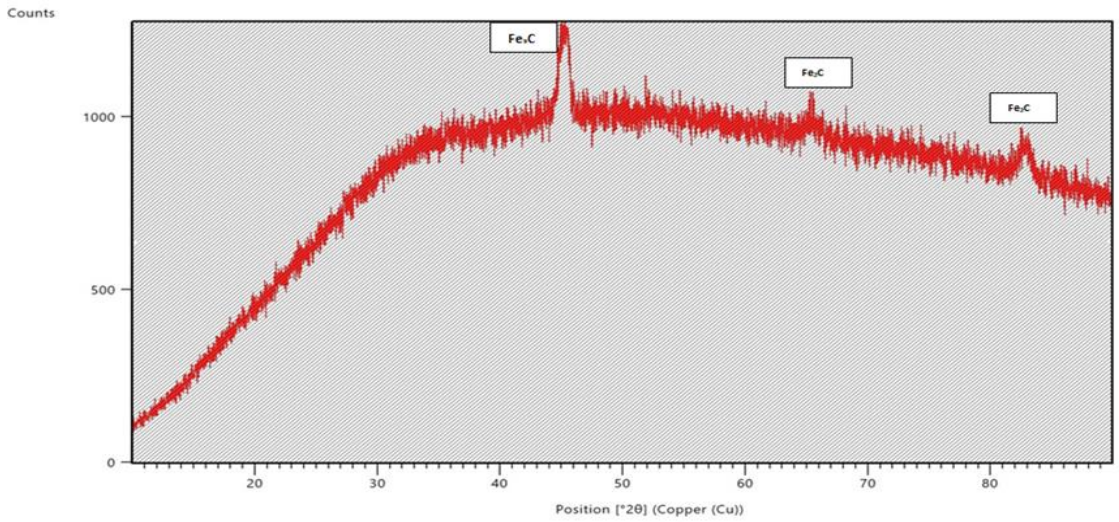

Figure 5.20. XRD results for sample (3) when Q =1.286(KJ/mm).

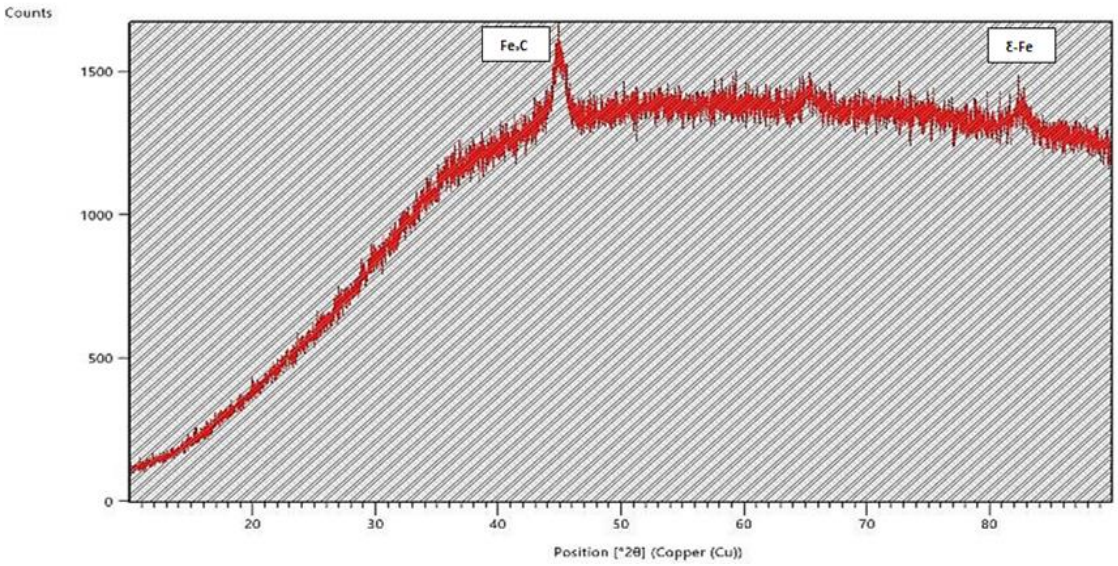

Figure 5.21. XRD results for sample (4) when Q =0.932(KJ/mm).

PART 6

CONCLUSION AND RECOMMENDATIONS

6.1. CONCLUSION

In summary, this study examined the impact of weld heat input on the mechanical characteristics and corrosion performance of weld joints using MIG welding methods in the specific context of petroleum storage tanks. The comprehensive analysis of these variables has yielded a number of significant findings that enhance the progress of welding requirements in relation to mechanical qualities and resistance to corrosion, as outlined below:

1. The connection between weld heat input and microstructure exhibited a notable level of statistical significance. Numerous empirical investigations have conclusively established a clear and direct relationship between fluctuations in heat input and the dimensions of both the heat-affected zone and the weld metal. The findings of this study indicate that an increased welding heat input leads to the formation of a more pronounced coarse grain structure, consistent with previous scholarly investigations. This observation underscores the extent of interdependence among these variables.
2. The utilization of microhardness testing yielded significant findings on the impact of heat input on the characteristics of the material. As the level of heat input was raised, there was a corresponding decrease in the microhardness values observed in the different weld zones. The emphasis on aligning with existing research highlights the significance of thoroughly evaluating heat input parameters to attain favorable microstructural properties and, as a result, improved microhardness.
3. The tensile test, which is widely regarded as a fundamental method for assessing material performance, has provided valuable insights into the

significant influence of heat input on the strength and flexibility of welding joints. By skillfully manipulating the velocity of motion and the amount of heat applied, the maximum tensile strength was attained. This statement emphasizes the significance of upholding precision in welding techniques and creates a clear relationship between heat input, fusion, and the overall strength of the joint.

4. The examination of corrosion resistance revealed the complex interaction among weld heat input, microstructure, and material choice. Attaining the necessary corrosion performance in components welded using the Metal Inert Gas (MIG) technique required careful consideration of welding settings and ensuring compatibility between the materials used. The results emphasize the necessity of adopting a comprehensive methodology towards the practice of welding.
5. The specimens comprise low-carbon steel, specifically plain carbon steel. The microstructure of this particular steel variant is composed of two primary constituents: ferrite, which is predominantly iron, and perlite, which is a composite of ferrite and cementite phases. The filler metal contains alloying elements as well as impurity elements, albeit in small quantities. These elements are not anticipated to be detectable in the X-ray diffraction (XRD) analysis. The anticipated phases in the XRD analysis include the pure iron phase and the cementite phase, as previously demonstrated.

6.2. RECOMMENDATIONS

This study offers various ideas and suggestions for future research, built upon the findings of the present study.

1. The substitution of the metal utilized in this investigation involved the incorporation of alternative metal varieties employed in the containment and storage of petroleum in tanks and vessels.
2. The examination of MIG welding techniques with pipeline infrastructure, as well as its application in the construction and maintenance of petroleum storage tanks.

3. The examination of the various dimensions of the petroleum storage tank's plate reveals a range of thicknesses.
4. The utilization of novel methodologies for assessing the corrosion resistance in diverse corrosive settings where petroleum storage tanks are situated.
5. To examine the influence of welding on mechanical properties and corrosion behavior, alternative welding techniques will be employed.

This thesis offers a comprehensive investigation into the intricate interplay among weld heat input, microstructure, mechanical properties, and corrosion performance in MIG-welded joints within the domain of petroleum storage tanks. The results underscore the importance of employing precise welding methods to ensure the enduring structural integrity of critical components in energy infrastructure, with notable consequences for the fabrication of petroleum storage tanks and the welding sector. The anticipation is that the ongoing advancement of welding techniques and their utilization will foster ingenuity and exceptional outcomes in the domains of material science and engineering, particularly when forthcoming investigations build upon prior findings.

REFERENCES

[1] G. C. da Silva Costa and A. A. de Resende, “Evaluation of the TIG–MIG/MAG welding process in direct polarity,” *SN Appl Sci*, vol. 2, no. 2, 2020, doi: 10.1007/s42452-020-1953-7.

[2] L. D. Meng, Q. Zhang, Y. L. Di, and W. Shen, “Research and Development of Precision MIG/MAG Welding,” *Adv Mat Res*, vol. 1095, pp. 824–827, 2015, doi: 10.4028/www.scientific.net/amr.1095.824.

[3] V. I. Safta, D. Mnerie, and G. V. Mnerie, “Some Peculiarities of MIG-MAG Welding Processes with Concentrated Energies,” *Key Eng Mater*, vol. 890, pp. 3–8, 2021, doi: 10.4028/www.scientific.net/kem.890.3.

[4] S. C. Azevedo and A. A. de Resende, “Effect of angle, distance between electrodes and TIG current on the weld bead geometry in TIG-MIG/MAG welding process,” *The International Journal of Advanced Manufacturing Technology*, vol. 114, no. 5–6, pp. 1505–1515, 2021, doi: 10.1007/s00170-021-07004-7.

[5] R. H. G. e Silva, J. C. Dutra, and R. Gohr, “Scientific and technological fundamentals for the development of the controlled short circuiting MIG/MAG welding process (CCC) – A review of the literature. Part 3 of 3: principles of controlled current short circuiting MIG/MAG systems,” *Welding International*, vol. 23, no. 4, pp. 251–260, 2009, doi: 10.1080/09507110802543393.

[6] Y. Al-Jubouri and M. Al-Hayali, “Geoeconomics of Pipelines Transporting Oil in the Arab Mashreq Countries,” *College Of Basic Education Research Journal*, vol. 16, no. 4, pp. 639–662, 2020, doi: 10.33899/berj.2020.167231.

[7] E. O. Ogundimu, E. T. Akinlabi, and M. F. Erinosho, “Comparative Study between TIG and MIG Welding Processes,” *J Phys Conf Ser*, vol. 1378, no. 2, p. 022074, 2019, doi: 10.1088/1742-6596/1378/2/022074.

[8] A. Kausar, “Study of Weld Quality characteristics of Tungsten Inert Gas Welding of Dissimilar Metals SS 316L and IS 2062 Plates,” *Int J Res Appl Sci Eng Technol*, vol. 7, no. 6, pp. 759–767, 2019, doi: 10.22214/ijraset.2019.6131.

[9] K. V. Mjali, A. Els-Botes, and P. M. Mashinini, “The efects of laser and mechanical forming on the hardness and microstructural layout of commercially pure grade 2 titanium alloy plates,” in *ASME 2017 12th International Manufacturing Science and Engineering Conference, MSEC 2017 collocated with the JSME/ASME 2017 6th International Conference on Materials and Processing*, 2017. doi: 10.1115/MSEC2017-2603.

[10] D. Bandhu and K. Abhishek, “Assessment of weld bead geometry in modified shortcircuiting gas metal arc welding process for low alloy steel,” *Materials and Manufacturing Processes*, vol. 36, no. 12, pp. 1384–1402, 2021, doi: 10.1080/10426914.2021.1906897.

[11] R. E. Avery and D. Parsons, “Welding stainless and 9% nickel steel cryogenic vessels,” *Welding Journal (Miami, Fla)*, vol. 74, no. 11, 1995.

[12] K. Sri Ram Vikas, K. S. Rao, Rahul, G. M. Reddy, and V. S. N. Venkata Ramana, “Influence of heat treatments on microstructural and mechanical properties of Grade 5 titanium friction welds,” *Engineering Research Express*, vol. 4, no. 2, p. 025053, 2022, doi: 10.1088/2631-8695/ac7a0a.

[13] J. H. Chujutalli, M. I. Lourenço, and S. F. Estefen, “Experimental-based methodology for the double ellipsoidal heat source parameters in welding simulations,” *Marine Systems & Ocean Technology*, vol. 15, no. 2, pp. 110–123, 2020, doi: 10.1007/s40868-020-00074-4.

[14] A. Karpagaraj, N. Rajesh Kumar, K. Sankaranarayanasamy, N. Siva Shanmugam, and M. Cheepu, “Simulation and Experimental Studies on Arc Efficiency and Mechanical Characterization for GTA-Welded Ti–6Al–4V Sheets,” *Arab J Sci Eng*, vol. 45, no. 11, pp. 9639–9650, 2020, doi: 10.1007/s13369-020-04876-x.

[15] M. P. Garcia, G. L. Mantovani, R. Vasant Kumar, and R. A. Antunes, “Corrosion Behavior of Metal Active Gas Welded Joints of a High-Strength Steel for Automotive Application,” *J Mater Eng Perform*, vol. 26, no. 10, pp. 4718–4731, 2017, doi: 10.1007/s11665-017-2900-7.

[16] S. Li, H. Dong, L. Shi, P. Li, and F. Ye, “Corrosion behavior and mechanical properties of Al-Zn-Mg aluminum alloy weld,” *Corros Sci*, vol. 123, pp. 243–255, 2017, doi: 10.1016/j.corsci.2017.05.007.

[17] R. A. ADEWUYI and J. O. AWEDA, “CHARACTERIZATION OF WELD HEAT INPUT EFFECTS ON MECHANICAL PROPERTIES OF Cr-Mo STEEL BAR USING TIG WELDING PROCESS,” *European Journal of Materials Science and Engineering*, vol. 6, no. 4, 2021, doi: 10.36868/ejmse.2021.06.04.192.

[18] E. Yılmaz and F. Fındık, “Effect of shielding gas on microstructure and mechanical properties in AA6061-T6 alloy MIG welding,” *Periodicals of Engineering and Natural Sciences (PEN)*, vol. 10, no. 1, p. 268, 2022, doi: 10.21533/pen.v10i1.2159.

[19] S. C. Moi, P. K. Pal, A. Bandyopadhyay, and R. Rudrapati, “Effect of Heat Input on the Mechanical and Metallurgical Characteristics of TIG Welded Joints,” *Journal of Mechanical Engineering*, vol. 16, no. 2, pp. 29–40, 2019, doi: 10.24191/jmeche.v16i2.15324.

[20] M. B. Chennaiah, P. Nanda Kumar, and K. Prahlada Rao, “Influence of Heat Input and PWHT on the Microstructure and Mechanical Properties in

Dissimilar (IS2062-EN8) Welded Joints," *Procedia Comput Sci*, vol. 85, pp. 54–61, 2016, doi: 10.1016/j.procs.2016.05.176.

[21] G. Mohammed, M. Ishak, S. Aqida, and H. Abdulhadi, "Effects of Heat Input on Microstructure, Corrosion and Mechanical Characteristics of Welded Austenitic and Duplex Stainless Steels: A Review," *Metals (Basel)*, vol. 7, no. 2, p. 39, 2017, doi: 10.3390/met7020039.

[22] A. H. Baghdadi, Z. Sajuri, A. Keshtgar, N. M. Sharif, and A. Rajabi, "Mechanical Property Improvement in Dissimilar Friction Stir Welded Al5083/Al6061 Joints: Effects of Post-Weld Heat Treatment and Abnormal Grain Growth," *Materials*, vol. 15, no. 1, 2022, doi: 10.3390/ma15010288.

[23] H. Qin, Y. Tang, and P. Liang, "Effect of Heat Input on Microstructure and Corrosion Behavior of High Strength Low Alloy Steel Welds," *Int J Electrochem Sci*, vol. 16, no. 4, p. 210449, 2021, doi: 10.20964/2021.04.07.

[24] H. A. Hussein, "Corrosion Behavior Evaluation of TIG Welding Joint of Low Carbon Steel," *Diyala Journal of Engineering Sciences*, vol. 13, no. 3, pp. 35–43, 2020, doi: 10.24237/djes.2020.13304.

[25] A. V Bansod and A. P. Patil, "Effect of Welding Processes on Microstructure, Mechanical Properties, and Corrosion Behavior of Low-Nickel Austenitic Stainless Steels," *Metallography, Microstructure, and Analysis*, vol. 6, no. 4, pp. 304–314, 2017, doi: 10.1007/s13632-017-0368-3.

[26] S. Geng, J. Sun, L. Guo, and H. Wang, "Evolution of microstructure and corrosion behavior in 2205 duplex stainless steel GTA-welding joint," *J Manuf Process*, vol. 19, pp. 32–37, 2015, doi: 10.1016/j.jmapro.2015.03.009.

[27] E. Evin and M. Tomáš, "Formability Prediction of Laser-Welded Stainless Steel AISI 304 and AISI 430," *Metals (Basel)*, vol. 12, no. 1, p. 54, 2021, doi: 10.3390/met12010054.

[28] A. Di Schino and C. Testani, "Corrosion Behavior and Mechanical Properties of AISI 316 Stainless Steel Clad Q235 Plate," *Metals (Basel)*, vol. 10, no. 4, p. 552, 2020, doi: 10.3390/met10040552.

[29] L. Michel, A. M. A. Sanchez, V. Silvestru, I. Ariza, A. Taras, and U. Angst, "Corrosion behaviour of point-by-point wire and arc additively manufactured steel bars," *Materials and Corrosion*, vol. 73, no. 7, pp. 996–1014, 2022, doi: 10.1002/maco.202112994.

[30] N. A. Abd Razak and S. S. Ng, "Investigation of Effects of MIG Welding on Corrosion Behaviour of AISI 1010 Carbon Steel," *JOURNAL OF MECHANICAL ENGINEERING AND SCIENCES*, vol. 7, pp. 1168–1178, 2014, doi: 10.15282/jmes.7.2014.16.0114.

[31] W. Xie and C. Yang, "Microstructure, mechanical properties and corrosion behavior of austenitic stainless steel sheet joints welded by gas tungsten arc (GTA) and ultrasonic–wave–assisted gas tungsten pulsed arc (U–GTPA),"

Archives of Civil and Mechanical Engineering, vol. 20, no. 2, 2020, doi: 10.1007/s43452-020-00044-y.

[32] G. Qin, Y. Su, and S. Wang, "Microstructures and properties of pulsed MIG arc brazed-fusion welded joint of al alloy and galvanized steel," *Jinshu Xuebao/Acta Metallurgica Sinica*, vol. 48, no. 8, 2012, doi: 10.3724/SP.J.1037.2012.00046.

[33] N. Çömez and H. Durmuş, "Corrosion behavior and mechanical properties of cold metal transfer welded dissimilar AA7075-AA5754 alloys," *J Cent South Univ*, vol. 27, no. 1, 2020, doi: 10.1007/s11771-020-4274-5.

[34] A. Gupta, A. Kumar, T. Baskaran, S. B. Arya, and R. K. Khatirkar, "Effect of Heat Input on Microstructure and Corrosion Behavior of Duplex Stainless Steel Shielded Metal Arc Welds," *Transactions of the Indian Institute of Metals*, vol. 71, no. 7, pp. 1595–1606, 2018, doi: 10.1007/s12666-018-1294-z.

[35] P. Saha, S. Datta, M. S. Raza, and D. K. Pratihar, "Effects of Heat Input on Weld-Bead Geometry, Surface Chemical Composition, Corrosion Behavior and Thermal Properties of Fiber Laser-Welded Nitinol Shape Memory Alloy," *J Mater Eng Perform*, vol. 28, no. 5, pp. 2754–2763, 2019, doi: 10.1007/s11665-019-04077-0.

[36] B.-S. Huang, J. Yang, D.-H. Lu, and W.-J. Bin, "Study on the microstructure, mechanical properties and corrosion behaviour of S355JR/316L dissimilar welded joint prepared by gas tungsten arc welding multi-pass welding process," *Science and Technology of Welding and Joining*, vol. 21, no. 5, pp. 381–388, 2016, doi: 10.1080/13621718.2015.1122152.

[37] S. M. Gan, Y. Q. Han, and X. Y. Bao, "Influence of Energy Ratio of Hybrid Heat Source on Residual Stress Distribution of 7A52 Aluminum Alloy VPPA-MIG Hybrid Welding," *Manufacturing Technology*, vol. 22, no. 3, pp. 279–287, 2022, doi: 10.21062/mft.2022.033.

[38] S. L. Lawal, S. A. Afolalu, T.-C. Jen, and E. T. Akinlabi, "Tungsten inert gas (TIG) and metal inert gas (MIG) welding applications - critical review," *E3S Web of Conferences*, vol. 390, p. 05012, 2023, doi: 10.1051/e3sconf/202339005012.

[39] Z. Du, K. Xu, L. Wang, X. Zhang, and X. Zhang, "Characterization of the local mechanical properties of 5083-5383 MIG welded joints," *J Phys Conf Ser*, vol. 2390, no. 1, p. 012013, 2022, doi: 10.1088/1742-6596/2390/1/012013.

[40] Budiarto, K. Turnip, and Hantariksa, "The effect of current gouging arc welding analysis of A283 Gr C steel to the tensile strength, hardness and microstructure," *IOP Conf Ser Mater Sci Eng*, vol. 420, p. 012055, 2018, doi: 10.1088/1757-899x/420/1/012055.

[41] L. O. Osoba, W. A. Ayoola, Q. A. Adegbuji, and O. A. Ajibade, "Influence of Heat Inputs on Weld Profiles and Mechanical Properties of Carbon and

Stainless Steel," *Nigerian Journal of Technological Development*, vol. 18, no. 2, pp. 135–143, 2021, doi: 10.4314/njtd.v18i2.8.

[42] S. Ahmed Albayati *et al.*, "Laser Cladding Treatment to Enhance the Corrosin Resistance and Surface Hardness by Electrophoretic Coatings to A283 Steel," *Diyala Journal of Engineering Sciences*, pp. 52–61, 2022, doi: 10.24237/djes.2022.15405.

[43] A. S. Alwan and S. K. Fayyadh, "Effect of welding heat input on corrosion rate of sprinkler irrigation piping joints by tig welding used in South of Iraq," *Iraqi Journal of Agricultural Sciences*, vol. 50, no. 1, 2019.

[44] C. Chen, G. Sun, W. Du, Y. Li, C. Fan, and H. Zhang, "Influence of heat input on the appearance, microstructure and microhardness of pulsed gas metal arc welded Al alloy weldment," *Journal of Materials Research and Technology*, vol. 21, pp. 121–130, Nov. 2022, doi: 10.1016/J.JMRT.2022.09.028.

[45] K. Weman, *Welding processes handbook*. 2003. doi: 10.1533/9781855738539.

[46] "Semiconductor & Flat Panel Display Inspection Microscopes | Olympus." Accessed: Nov. 01, 2023. [Online]. Available: https://www.olympus-ims.com/en/microscope/mx/

[47] *Principles of Metal Manufacturing Processes*. 1999. doi: 10.1016/b978-0-340-73162-8.x5000-0.

[48] D. K. Dwivedi, "Weldability of Metals: Characteristics of Metals and Weldability," in *Fundamentals of Metal Joining*, 2022. doi: 10.1007/978-981-16-4819-9_29.

[49] C. B. Dallam and B. K. Damkroger, "Characterization of Welds," *Weld Integrity and Performance*, pp. 39–55, Jul. 2022, doi: 10.31399/ASM.TB.WIP.T65930039.

[50] *Weld Integrity and Performance*. 1997. doi: 10.31399/asm.tb.wip.9781627083591.

[51] "Weldability." Accessed: Nov. 01, 2023. [Online]. Available: https://www.weldability-sif.com/

[52] S. A. David, S. S. Babu, and J. M. Vitek, "Welding: Solidification and microstructure," *JOM*, vol. 55, no. 6, pp. 14–20, 2003, doi: 10.1007/s11837-003-0134-7.

[53] S. Richard, *The procedure handbook of arc welding*. 1995.

[54] S. Kou, *Welding Metallurgy*. 2002. doi: 10.1002/0471434027.

[55] P. Liao, H. Wan, J. Min, K. Zhang, and J. Lin, "Experimental study on heat-affected zones of aluminum alloys in flow drill riveting," *Journal of Materials Research and Technology*, vol. 18, 2022, doi: 10.1016/j.jmrt.2022.03.044.

[56] Z. Wang *et al.*, “Revealing Charpy Impact Toughness Variations of EH36 Shipbuilding Steel Weld Metals Processed by CaF2-Al2O3-TiO2 Fluxes under High Heat Input Submerged Arc Welding,” *J Mater Eng Perform*, 2023, doi: 10.1007/s11665-023-08168-x.

[57] J. A. Shields, “The Physical Metallurgy of Steels,” *Nucl Technol*, vol. 59, no. 1, 1982, doi: 10.13182/nt82-a33065.

[58] M. Fitri, B. Sukiyono, and M. L. Simanjuntak, “Pengaruh Waktu Penahanan pada Perlakuan Panas Paska Pengelasan terhadap Ketangguhan Sambungan Las Baja,” *SINTEK JURNAL: Jurnal Ilmiah Teknik Mesin*, vol. 13, no. 2, 2019, doi: 10.24853/sintek.13.2.80-86.

[59] W. Zhang, G. G. Roy, J. W. Elmer, and T. DebRoy, “Modeling of heat transfer and fluid flow during gas tungsten arc spot welding of low carbon steel,” *J Appl Phys*, vol. 93, no. 5, pp. 3022–3033, 2003, doi: 10.1063/1.1540744.

[60] “AWS Bookstore.” Accessed: Nov. 01, 2023. [Online]. Available: https://pubs.aws.org/

[61] A. I S and E. E, “Effect of Arc Welding Current on the Mechanical Properties of A36 Carbon Steel Weld Joints,” *International Journal of Mechanical Engineering*, vol. 2, no. 9, pp. 32–40, 2015, doi: 10.14445/23488360/ijme-v2i9p113.

[62] H. Nurdin, P. Purwantono, and K. Umurani, “Tensile strength of welded joints in low carbon steel using metal inert gas (MIG) welding,” *INVOTEK: Jurnal Inovasi Vokasional dan Teknologi*, vol. 21, no. 3, pp. 175–180, 2021, doi: 10.24036/invotek.v21i3.934.

[63] M. Sarkari Khorrami, M. A. Mostafaei, H. Pouraliakbar, and A. H. Kokabi, “Study on microstructure and mechanical characteristics of low-carbon steel and ferritic stainless steel joints,” *Materials Science and Engineering: A*, vol. 608, pp. 35–45, 2014, doi: 10.1016/j.msea.2014.04.065.

[64] A. B. Spierings, K. Dawson, K. Kern, F. Palm, and K. Wegener, “SLM-processed Sc- and Zr- modified Al-Mg alloy: Mechanical properties and microstructural effects of heat treatment,” *Materials Science and Engineering: A*, vol. 701, pp. 264–273, 2017, doi: 10.1016/j.msea.2017.06.089.

[65] G. Cornacchia, S. Cecchel, and A. Panvini, “A comparative study of mechanical properties of metal inert gas (MIG)-cold metal transfer (CMT) and fiber laser-MIG hybrid welds for 6005A T6 extruded sheet,” *The International Journal of Advanced Manufacturing Technology*, vol. 94, no. 5–8, pp. 2017–2030, 2017, doi: 10.1007/s00170-017-0914-9.

[66] E. Maldonado-Bandala *et al.*, “Corrosion Behavior of AISI 1018 Carbon Steel in Localized Repairs of Mortars with Alkaline Cements and Engineered Cementitious Composites,” *Materials (Basel)*, vol. 13, no. 15, p. 3327, Jul. 2020, doi: 10.3390/ma13153327.

RESUME

Hyder Abed Alrazzaq Ajeel AL-ETHAWI, a mechanical engineer, graduated from the university of Technology in Baghdad –Iraq and obtained a bachelor's degree in 2006. Worked in mechanical engineering in several locations, currently studying for a master's degree at Karabük University in mechanical engineering.